

THICK-DISK EVOLUTION INDUCED BY THE GROWTH OF AN EMBEDDED THIN DISK

ÁLVARO VILLALOBOS,^{1,2} STELIOS KAZANTZIDIS,³ AND AMINA HELMI¹

The Astrophysical Journal, accepted

ABSTRACT

We perform collisionless N -body simulations to investigate the evolution of the structural and kinematical properties of simulated thick disks induced by the growth of an embedded thin disk. The thick disks used in the present study originate from cosmologically-common 5:1 encounters between initially-thin primary disk galaxies and infalling satellites. The growing thin disks are modeled as static gravitational potentials and we explore a variety of growing-disk parameters that are likely to influence the response of thick disks. We find that the final thick-disk properties depend strongly on the total mass and radial scale-length of the growing thin disk, and much less sensitively on its growth timescale and vertical scale-height as well as the initial sense of thick-disk rotation. Overall, the growth of an embedded thin disk can cause a substantial contraction in both the radial and vertical direction, resulting in a significant decrease in the scale-lengths and scale-heights of thick disks. Kinematically, a growing thin disk can induce a notable increase in the mean rotation and velocity dispersions of thick-disk stars. We conclude that the reformation of a thin disk via gas accretion may play a significant role in setting the structure and kinematics of thick disks, and thus it is an important ingredient in models of thick-disk formation.

Subject headings: cosmology: dark matter — cosmology: theory — galaxies: formation — galaxies: kinematics and dynamics — galaxies: structure — methods: numerical

1. INTRODUCTION

Hierarchical models of cosmological structure formation, such as the currently favored cold dark matter (CDM) paradigm (e.g., White & Rees 1978; Blumenthal et al. 1984), generically predict that galaxies are built via the continuous accretion of smaller systems. Indeed, a growing body of observational evidence has recently confirmed this prediction with the discovery of tidal streams and complex stellar structures in the Milky Way (MW) (e.g., Ibata et al. 1994; Helmi et al. 1999; Yanny et al. 2000; Ibata et al. 2001b; Newberg et al. 2002; Majewski et al. 2003; Martínez-Delgado et al. 2005; Belokurov et al. 2006), the Andromeda galaxy (Ibata et al. 2001a; Ferguson et al. 2002, 2005; Kalirai et al. 2006; Ibata et al. 2007), and beyond the Local Group (e.g., Malin & Hadley 1997; Shang et al. 1998; Peng et al. 2002; Forbes et al. 2003; Pohlen et al. 2004).

In the context of CDM, bombardment by infalling satellites may lead to the heating of thin galactic disks and the subsequent formation of thick disks (e.g., Quinn & Goodman 1986; Walker et al. 1996; Velázquez & White 1999; Hayashi & Chiba 2006; Villalobos & Helmi 2008, hereafter Paper I; Kazantzidis et al. 2008; Read et al. 2008), and can even cause thin-disk destruction (Purcell et al. 2009). Depending on when the most substantial accretion event has occurred, a new thin disk may reform, for example, via the cooling of hot gas in the galactic halo (e.g., White & Rees 1978; Mo et al. 1998; Baugh 2006) and be observable at present.

In this scenario, the dynamical effects of the cooling gas

on the properties of the post-accretion thickened stellar distribution could be significant. Indeed, as the gas cools down and slowly accumulates at the center of the system, it can induce concomitant contraction of the heated stellar component due to its gravity (see e.g., Elmegreen & Elmegreen 2006; Kazantzidis et al. 2009). This phenomenon is similar in spirit to the contraction of dark matter halos during the process of baryonic cooling that leads to the formation of galaxies (e.g., Zeldovich et al. 1980; Barnes & White 1984; Blumenthal et al. 1986).

Significant theoretical effort, including both semi-analytic modeling (Tóth & Ostriker 1992; Benson et al. 2004; Hopkins et al. 2008) and numerical simulations (Quinn & Goodman 1986; Quinn et al. 1993; Walker et al. 1996; Huang & Carlberg 1997; Sellwood et al. 1998; Velázquez & White 1999; Font et al. 2001; Ardi et al. 2003; Gauthier et al. 2006; Hayashi & Chiba 2006; Kazantzidis et al. 2008; Read et al. 2008; Purcell et al. 2009; Kazantzidis et al. 2009; Moster et al. 2009) has been devoted to exploring the dynamical heating of galactic disks via satellite accretion events. However, very few studies have investigated the response of the resulting thickened stellar component to the gas accumulation and subsequent reformation of a thin-disk (see, however, Kazantzidis et al. 2009; Moster et al. 2009). A full model of satellite-disk interactions in a cosmological context including gas dynamics and star formation would be ideal to obtain a complete picture of this physical process. Unfortunately, due to the fact that they are highly complex and very costly in terms of computational power, cosmological simulations that could address in a systematic way the structural and kinematical evolution of thick disks in response to growing thin-disks do not yet exist.

Recently, Kazantzidis et al. (2009) performed dissipationless N -body simulations to investigate the influence of a slowly growing thin disk on the properties of an initially-thick galactic disk. These authors considered three models of growing disks with masses equal to 10%, 50%, and 100%

¹ Kapteyn Astronomical Institute, University of Groningen, P.O. Box 800, 9700 AV Groningen, The Netherlands; villalobos, ahelmi@astro.rug.nl.

² Present address: INAF-Osservatorio Astronomico di Trieste, Via Tiepolo 11, I-34143 Trieste, Italy; villalobos@oats.inaf.it.

³ Center for Cosmology and Astro-Particle Physics; and Department of Physics; and Department of Astronomy, The Ohio State University, 191 West Woodruff Avenue, Columbus, OH 43210, USA; stelios@mps.ohio-state.edu.

of the mass of the thick disk, and showed that the latter contracted vertically as well as radially in response to the growth of the thin-disk component. Not unexpectedly, the magnitude of the thick-disk structural evolution was found to depend sensitively on the total mass of the growing disk. However, Kazantzidis et al. (2009) focused on a fairly small region of parameter space and, in addition, they utilized a fully-formed thick-disk galaxy instead of a galactic model whose thick disk formed self-consistently by encounters between an initially-thin disk and infalling satellites.

In the present paper, we expand upon this initiative by performing a *systematic* numerical study aiming to elucidate the effects of growing thin disks on both the morphology and kinematics of realistic thick disks. For the latter, we adopt a subset of the models presented in Paper I. Given the complex interplay of effects (e.g., gas cooling, star formation) relevant to the formation and evolution of spiral galaxies and the outstanding issues regarding disk galaxy formation in CDM cosmogonies (e.g., Mayer et al. 2008), we restrict ourselves to modeling the gravitational potential of a thin disk that slowly grows in mass over time using an ensemble of collisionless N -body simulations.

Our simulation set is carefully designed to permit an investigation of a large parameter space and we explore several aspects of the growth of a thin disk that are likely to have an effect on the morphological and kinematical evolution of thick disks. In particular, we vary the growth timescale, final mass, scale-length, scale-height, and orientation of the growing disk total angular momentum vector. In addition, we perform experiments where the same thin disk grows inside thick disks that rotate in either a prograde or retrograde sense with respect to their halos. The present work establishes that the reformation of a thin disk may play a significant role in setting the structural and kinematic properties of thick-disk stars, and thus it is an important ingredient in models of thick-disk formation.

The outline of this paper is as follows. In Section 2 we briefly describe the models adopted and the setup of the numerical experiments performed in the present study. Section 3 contains the results regarding the thick-disk morphological and kinematical evolution induced by the growth of a thin-disk component. A detailed comparison between the properties of the initial and post-growth thick disks is presented in Section 4. Lastly, Section 5 summarizes our main conclusions. Throughout this work we use the terms “thick disk” and “heated disk” interchangeably to indicate the perturbed stellar component that resulted from the original interaction between a thin primary disk galaxy and an infalling satellite, and consists of stars from both the stellar disk of the primary galaxy and the disrupted system.

2. METHODS

We begin this section by briefly describing the primary disk models used in this study. In Section 2.2 we introduce the thin-disk models and discuss the method we employ to grow them inside the thick disks. Lastly, in Section 2.3 we present the numerical experiments with growing disks of the adopted simulation campaign.

2.1. Models of Thick Disks

In Paper I, 25 dissipationless N -body simulations were carried out to study the general properties of thick disks formed by single encounters between a primary thin disk galaxy and a massive satellite system. These simulations explored: (1) two

models for the primary disk galaxy, whose structure and kinematics resembled those of the MW at present (“ $z=0$ ” experiments) and at $z=1$ (“ $z=1$ ” experiments); (2) two morphologies for the stellar component of the satellite, spherical and disk; (3) two mass ratios between the satellite and the primary disk galaxy (10% and 20%); and (4) three initial satellite orbital inclinations ($i = 0^\circ, 30^\circ$, and 60°), in both prograde and retrograde directions with respect to the rotation of the primary disk.

Both the primary disk galaxy and the satellite were initialized as “live” N -body models consisting of a dark matter and a stellar component. The dark halos of both systems followed the Navarro et al. (1997) density profile and have been adiabatically contracted to account for the presence of the stellar component (see e.g., Blumenthal et al. 1986; Mo et al. 1998). The stellar component of the spherical satellite was set up with structure and kinematics consistent with the observed fundamental plane of dE+dSphs galaxies (de Rijcke et al. 2005). On the other hand, the disk satellites have been constructed in the same way as the primary disk galaxies. Their scale-lengths and scale-heights are smaller than those of the primary disks, following the proportion between the virial radii of the corresponding dark matter halos (see Paper I for details). The orbital parameters of the encounters were drawn from studies of infalling substructures in a cosmological context (Benson 2005, see also Tormen 1997; Khochfar & Burkert 2006), and the satellites were released far away from the centers of the disk galaxies, ~ 35 (~ 50) times the disk scale-length for “ $z=0$ ” (“ $z=1$ ”) experiments.

The simulations of thick-disk formation were evolved for 5 Gyr (4 Gyr) in the “ $z=0$ ” (“ $z=1$ ”) experiments and the satellites have typically merged by $t = 3$ Gyr ($t = 2$ Gyr). By the final time, the systems are relaxed. The simulations were carried out with 5×10^5 particles in the host dark matter halo, and 10^5 particles in each of all the other components. The softenings of thick-disk stars range from 12 pc to 70 pc (we refer the reader to Paper I for a complete description of the experiments), and the softening of growing disk particles correspond to 1/5 of the growing disk scale-height (see Section 2.3).

The primary aim of the present work is to study the most generic features of the evolution of thick disks in response to the growth of an embedded thin disk. For this reason, we select a subset of the thick-disk models presented in Paper I (see Section 2.3 below). In particular, we focus on models that were produced via an encounter with a satellite on a low/intermediate orbital inclination. Assuming a dynamical heating model for the origin of thick disks (e.g. Kazantzidis et al. 2008), such accretion events are relevant to the formation of the thick disk of the MW (Paper I). This is based on the possible existence of a vertical gradient in the rotational velocity of the Galactic thick disk and on the observed value of σ_z/σ_R in the solar neighborhood (e.g. Girard et al. 2006; Vallenari et al. 2006). In addition, due to the fact that satellite structure is not essential in establishing the structural properties of thick disks (Paper I), we only consider thick-disk models that were produced by interactions with spherical satellites.

2.2. Models of Growing Disks

The growing disks follow an exponential distribution in cylindrical radius R , and their vertical structure is modeled in the standard way as a collection of isothermal sheets (Spitzer

TABLE 1
SUMMARY OF NUMERICAL EXPERIMENTS

Run (1)	M_d/M_{thick} (2)	Growing thin disk			alignment (6)	Thick disk	
		R_d (kpc) (3)	z_d (pc) (4)	τ (Gyr) (5)		rotation (7)	inclination (8)
Reference model	5	3	125	1	halo	prograde	30°
A1	5	3	125	1	halo	prograde	0°
A2	5	3	125	1	halo	prograde	60°
B1	5	3	125	0	halo	prograde	30°
B2	5	3	125	5	halo	prograde	30°
C1	2	3	125	1	halo	prograde	30°
C2	5	3	25	1	halo	prograde	30°
C3	5	1	125	1	halo	prograde	30°
D	5	3	125	1	thick disk	prograde	30°
E1	5	3	125	1	halo	prograde	0°
E2	5	3	125	1	halo	retrograde	0°

NOTES.— Column (1): Labels for the numerical simulations. Column (2): Mass of the growing thin disk in units of the initial thick disk. Column (3): Radial scale-length of the growing thin disk in kpc. Column (4): Vertical scale-height of the growing thin disk in pc. Column (5): Growth timescale of the thin disk in Gyr. Column (6): Alignment of the rotation axis of the growing thin disk. Column (7): Sense of rotation of the thick disk with respect to its halo. Column (8): Initial orbital inclination of the infalling satellite that produced the initial thick disk.

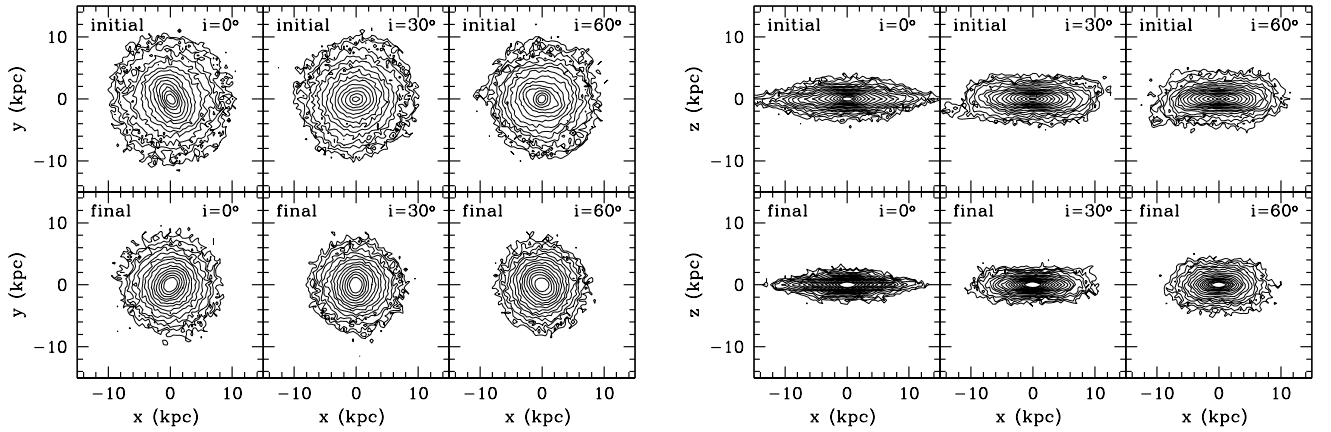


FIG. 1.— Initial (upper panels) and final (bottom panels) surface brightness contours of thick-disk stars viewed face-on (left panels) and edge-on (right panels) in the simulations with growing thin disks. Results are presented for experiment A with a thin-disk growth timescale of $\tau = 1$ Gyr and the orbital inclination of the accretion event that formed the initial heated disk is indicated in each panel. Contours correspond to equal surface brightness levels (0.39 mag arcsec⁻²) in the V-band for face-on (20.25–25.35 mag arcsec⁻²) and edge-on (19.09–25.35 mag arcsec⁻²) views. Thick disks experience strong radial and vertical contraction in response to the growth of a new thin disk component.

1942):

$$\rho_{\text{thin}}(R, z) = K \exp\left(-\frac{R}{R_d}\right) \text{sech}^2\left(\frac{z}{2z_d}\right), \quad (1)$$

where M_d , R_d , z_d denote the mass, radial scale-length, and (exponential) vertical scale-height of the disk, respectively, and $K = M_d/8\pi R_d z_d$.

Each growing-disk simulation was performed using the following procedure: (1) insert a *massless* Monte Carlo particle realization of the desired disk model inside the primary disk galaxies. (2) increase the mass of this distribution to its final value linearly over a timescale τ , according to the following law:

$$M(t) = M_d(t/\tau) \quad 0 \leq t \leq \tau. \quad (2)$$

During the growth period, the growing disk remains rigid and their particles are fixed in place (i.e., behaving like a fixed disk potential), while the “live” particles composing the thick disk and its dark matter halo are allowed to achieve equilibrium as the mass of the system grows. Throughout the experiments, all other properties of the growing disk (e.g., scale-length, scale-height) are kept constant. All numerical simulations of growing disks were carried out with the multi-stepping, parallel, tree N -body code PKDGRAV (Stadel 2001).

2.3. Numerical Experiments with Growing Disks

Overall, we have performed 11 simulations of the growth of a new thin disk within a subset of the thick disks presented

in Paper I. We have explored a variety of parameters related to the growing disks that may affect the thick-disk evolution, including: (1) the growth timescale: $\tau = 0$ Gyr, 1 Gyr, and 5 Gyr⁴; (2) the final mass: $M_d = 2M_{\text{thick}}$ and $5M_{\text{thick}}$, where M_{thick} denotes the mass of the initial thick disk⁵; (3) the vertical scale-height: $z_d = 25$ pc and 125 pc⁶; (4) the radial scale-length: $R_d = 1$ kpc and 3 kpc; (5) the orientation of the angular momentum vector: aligned either to the angular momentum of the dark matter halo or to the angular momentum vector of the thick disk; and (6) the sense of rotation of the initial thick disk with respect to its halo: prograde or retrograde. Lastly, we also compare the evolution of initial thick disks produced by infalling satellites on different orbital inclinations, $i = 0^\circ$, 30° , and 60° .

The runs are labeled as A, B, C, D, and E and summarized in Table 1. Our reference model is characterized by the following set of parameters for the growing thin disk: $\tau = 1$ Gyr, $M_d = 5M_{\text{thick}}$, $z_d = 125$ pc, $R_d = 3$ kpc, and a thick disk that is the result of a (prograde) satellite accretion event with an initial orbital inclination of $i = 30^\circ$. In what follows, we refer to experiment “X” to denote comparisons between Run “X” and the reference model, except for run E.

All numerical experiments of growing disks correspond to a total time of $t = \tau + 0.5$ Gyr (except for the case of instantaneous growth which is evolved for 1.5 Gyr to match the simulations with a growth timescale of $\tau = 1$ Gyr). Apart from the production simulations described above, we performed two additional sets of experiments. First, we evolved a subset of the initial thick disks in isolation for 1.5 Gyr and confirmed that their properties remained fairly unmodified. Second, after the full growth of the new thin disks, we evolved the resulting composite disk galaxies for another 4 Gyr in isolation, confirming that their properties do not evolve appreciably with time. Therefore, we conclude that the evolution of the thick-disks structural and kinematic properties presented next is due solely to the adiabatic compression caused by the growth of the thin disks.

3. RESULTS

3.1. Structural Evolution of Thick Disks

3.1.1. General Features

In general, the growth of a new thin disk induces three characteristic structural changes in all initial thick disks. First, it causes significant contraction in both the radial and vertical direction. Figure 1 focuses on experiment A and shows initial and final surface brightness contours of thick-disk stars viewed both face-on and edge-on. We stress that no stars from the growing thin disks are included in this analysis. The fact that the final contours appear much closer together and significantly less extended in the outer regions illustrates the con-

traction experienced by the disk stars. At the same brightness level, the innermost contours of the final systems are more extended compared to those of the initial ones. This indicates that the surface brightness associated with the central regions of the final systems increases. It is also important to note that the face-on surface brightness contours become rounder after the growth of the thin disk. This confirms results of earlier studies regarding the effects of baryonic dissipation on the shapes of dark matter halos (e.g., Dubinski 1994; Kazantzidis et al. 2004).

Figure 2 compares for the same experiment the initial radial positions of initial heated-disk stars to those after the growth of the new thin disk. Only stars within $R < 15$ kpc and $|z| < 1$ kpc in the final contracted thick disks are included in this analysis. The figure shows that the relation between initial and final radius is remarkably linear in all cases with practically the same slopes, regardless of the initial orbital inclination of the infalling satellite. In addition, the structural contraction induces a significant migration of thick-disk stars inwards. Indeed, stars that were initially located at $R \sim 14$ kpc end up at $R \sim 8$ kpc after the growth of the thin disk.

The angular momenta of individual thick disk particles are well conserved after the growth of the new thin disk, as it is shown in Figure 3 for experiment A1. In general this is found in all experiments, except in B1, as it is expected given its non-adiabatic nature. Particles within $R < 3$ kpc present a less clear conservation of their angular momenta, which is probably due to the exchange of angular momentum between halo particles and thick disk particles in the inner region.

The second common feature seen in all experiments is that the cold components present in the initial heated disks (see Paper I) are preserved after the thin-disk growth. As we discuss in the next section, the mass fraction associated with these components remains below $\sim 25\%$ of the total mass of the heated disks in all experiments. In principle, these thin components could represent old thin-disk populations given their similar spatial distribution and kinematics.

As discussed in Paper I, the satellite accretion events which produce the thick disks create flares in the outer regions of the primary disk galaxies (see also Kazantzidis et al. 2008). However, in spite of such flares, it was also found that (radially integrated) vertical surface brightness profiles of thick disks are very well represented by two sech^2 components. Another common characteristic to all experiments described here is the fact that the growth of a new thin disk also changes the vertical structure of thick disks, especially in the outer regions. The relevant analysis is presented in Figure 4 which shows results for run A1. This figure compares the final vertical surface brightness profile (integrated for $R < 10$ kpc) of the contracted thick disk to that of the initial thick disk evolved in isolation (for the same amount of time), and demonstrates that they are fairly different. More specifically, the growth of the thin disk causes the vertical surface brightness profiles to become substantially narrower (a closer inspection shows a significant contribution of satellite stars in the region $|z| > 1.5$ kpc, especially at larger radii). While a two-component sech^2 decomposition provides an accurate description of the vertical structure of the initial thick disk down to fairly low surface brightnesses, the growth of the new thin disk highlights the need for a more complicated functional form to describe the final vertical disk structure at large heights.

3.1.2. Experiments from A to E

⁴ Note that these values bracket the range of potential timescales for the disk growth including strongly non-adiabatic and adiabatic ones. While adopting an instantaneous growth for the disk is obviously unphysical, it still represents an interesting limiting case for the disk growth timescale.

⁵ Note that the value of $M_d = 2M_{\text{thick}} = 2.8 \times 10^{10} M_\odot$ is within the range of the total gas mass accreted by the MW disk since $z \sim 1$ ($1.5 - 3 \times 10^{10} M_\odot$) assuming a constant infall rate of $2 - 4 M_\odot/\text{yr}$ according to analytical models for the evolution of the MW disk in a cosmological context (Naab & Ostriker 2006). Although there are still large uncertainties in this estimate, the larger value of $M_d = 5M_{\text{thick}}$ is relevant to a system whose thin-thick mass ratio is similar to that of the Galaxy at present (e.g., Jurić et al. 2008).

⁶ Note that these values are consistent with the scale-heights of known, young, star-forming disks observed both in external galaxies (e.g., Wainscoat et al. 1989; Matthews 2000) and in the MW (e.g., Bahcall & Soneira 1980; Reid & Majewski 1993).

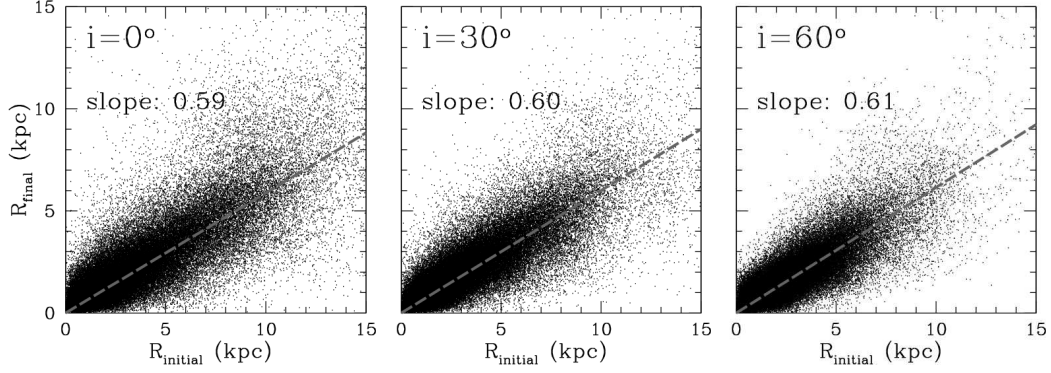


FIG. 2.— Initial and final cylindrical radial distance of heated disk stars before and after the structural contraction. Results are presented for experiment A. The dashed line shows the best linear fit. For clarity, only heated disk stars are shown.

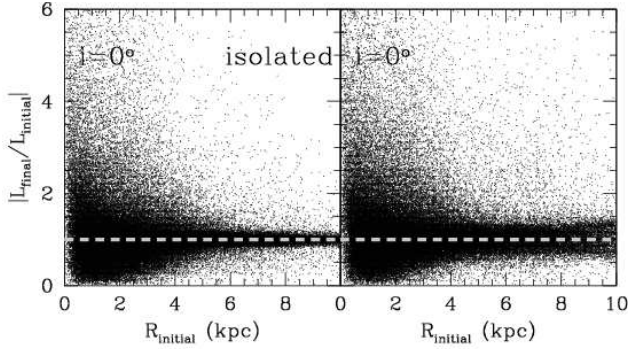


FIG. 3.— Ratio of final-to-initial angular momenta of particles belonging to the isolated thick disk (i.e., evolved without the growing new thin disk) (left panel) and the corresponding contracted thick disk in experiment A1 (right panel). In both cases the thick disks have been evolved for the same amount of time. The dashed line indicates where $|L_{\text{final}}/L_{\text{initial}}| = 1$.

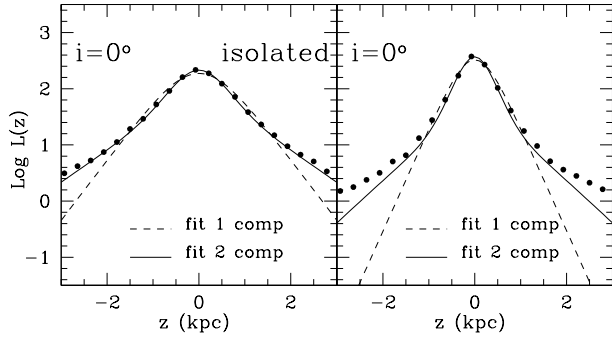


FIG. 4.— Final vertical surface brightness profiles of the isolated thick disk (i.e., evolved without the growing new thin disk) (left panel) and the corresponding contracted thick disk in run A1 (right panel). The former has been evolved in isolation for the same amount of time as the latter and profiles are obtained via integrating within $R < 10$ kpc. Dashed and solid lines show results for the best-fit with one- and two-component sech^2 decompositions, respectively. The growth of a new thin disk induces changes to the vertical structure of the initial thick disks, highlighting the need for a more complicated functional form to describe the final disk structure at large heights.

Figures 5 to 11 present results for all experiments from A to E. In particular, these figures show (1) the vertical surface brightness profiles of the thick disks at various projected radii (including the best two-components sech^2 fits) before and after the growth of the new thin disk; (2) the surface density de-

composition (into cold/thinner and hot/thicker components) of the final thick disks, including the parts of the profiles considered to estimate the respective scale-lengths and the mass fraction associated with the cold component; and (3) a comparison between scale-lengths and scale-heights of thick disks (for cold and hot components) before and after the growth of the new thin disk. All of these properties are computed within $R < 10$ kpc and $|z| < 4$ kpc. Lastly, unless otherwise explicitly stated, we do not include stars from the growing thin disks in the analysis presented below.

Briefly, the decomposition of the vertical surface brightness profiles is obtained by fitting, at equally spaced projected radii on the (properly aligned) thick disks, the function $L(z) = L_1 \text{sech}^2(z/2z_1) + L_2 \text{sech}^2(z/2z_2)$, where L_i and z_i are the local brightness on the plane and local scale-heights, respectively, and both are free parameters (although in general $z_1 < z_2$). In these fits, stars from both the disk and the (disrupted) satellite are included within the spatial range mentioned above. For each thick disk one global scale-height per component is finally obtained by averaging the local scale-heights over all radii, weighting by the local brightness on the plane. On the other hand, the decomposition of the surface density profiles of thick disks is obtained by simply considering the region $0 < |z| < 0.5z_1$ as dominated by the cold/thinner component, and the region $z_1 < |z| < 4$ kpc as dominated by the hot/thicker component. Finally, the scale-lengths of each component are computed by applying a linear fit to $\ln \Sigma(R)$, avoiding non-axisymmetries associated to both the central regions and the very outskirts. For more details, we refer the reader to Paper I.

Experiment A (Figure 5) shows that the final mass fraction associated to the cold component is larger than the initial one for thick disks formed after an either low or intermediate inclination merger ($i = 0^\circ - 30^\circ$), as opposite to the case when the thick disk is formed after a high inclination merger ($i = 60^\circ$), where the final mass fraction is smaller than the initial one. It is also found that in an absolute sense the final mass fraction associated to the cold component remains within the range $\sim 14\text{--}20\%$, as before the growth of the new disk. The exception is the $i = 60^\circ$ case in which the mass of the cold remnant may amount up to 50% of that of the initial cold component. This fraction however is relatively poorly determined because it depends strongly on the region selected to fit the exponential profile to the surface density which appears to show a change of slope around $R \sim 4$ kpc.

Experiment B (Figure 6) shows that the thick-disk structural

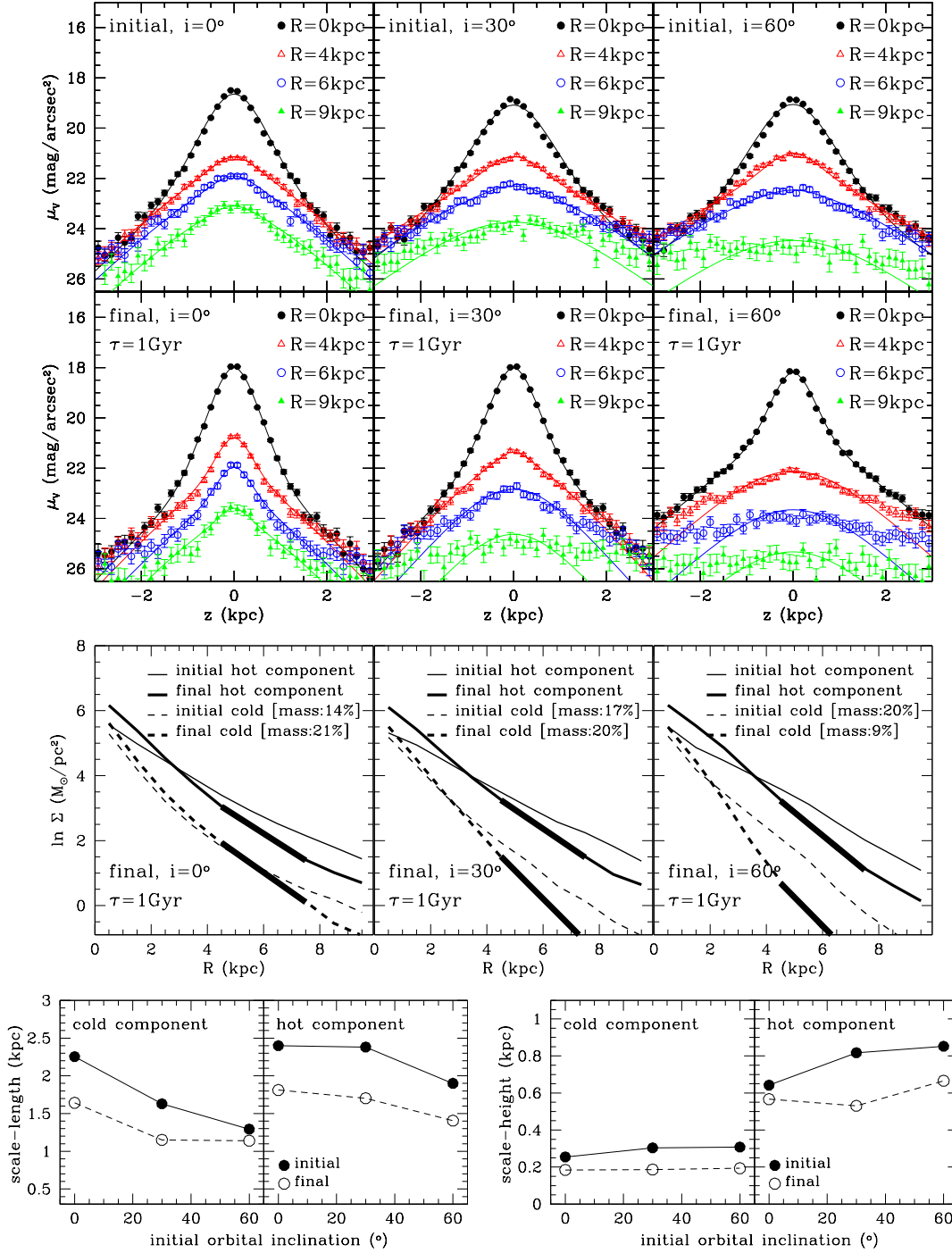


FIG. 5.— Experiment A. Final thick-disk properties induced by the growth of the fiducial thin disk on a timescale of $\tau = 1$ Gyr. The initial thick disks were formed by satellite accretion events with initial orbital inclinations of $i = 0^\circ$ (left panels), $i = 30^\circ$ (middle panels), and $i = 60^\circ$ (right panels). From top to bottom: Rows 1 and 2 show the initial and final vertical surface brightness profiles of the thick disks. Row 3 shows results for final thick-disk surface density profiles decomposed into a “cold” and a “hot” component. The mass fractions associated with these components are indicated in each panel. Row 4 presents initial (filled symbols) and final (open symbols) scale-lengths and scale-heights for the “cold” and “hot” components as a function of the orbital inclination of the encounter that produced the initial thick disks.

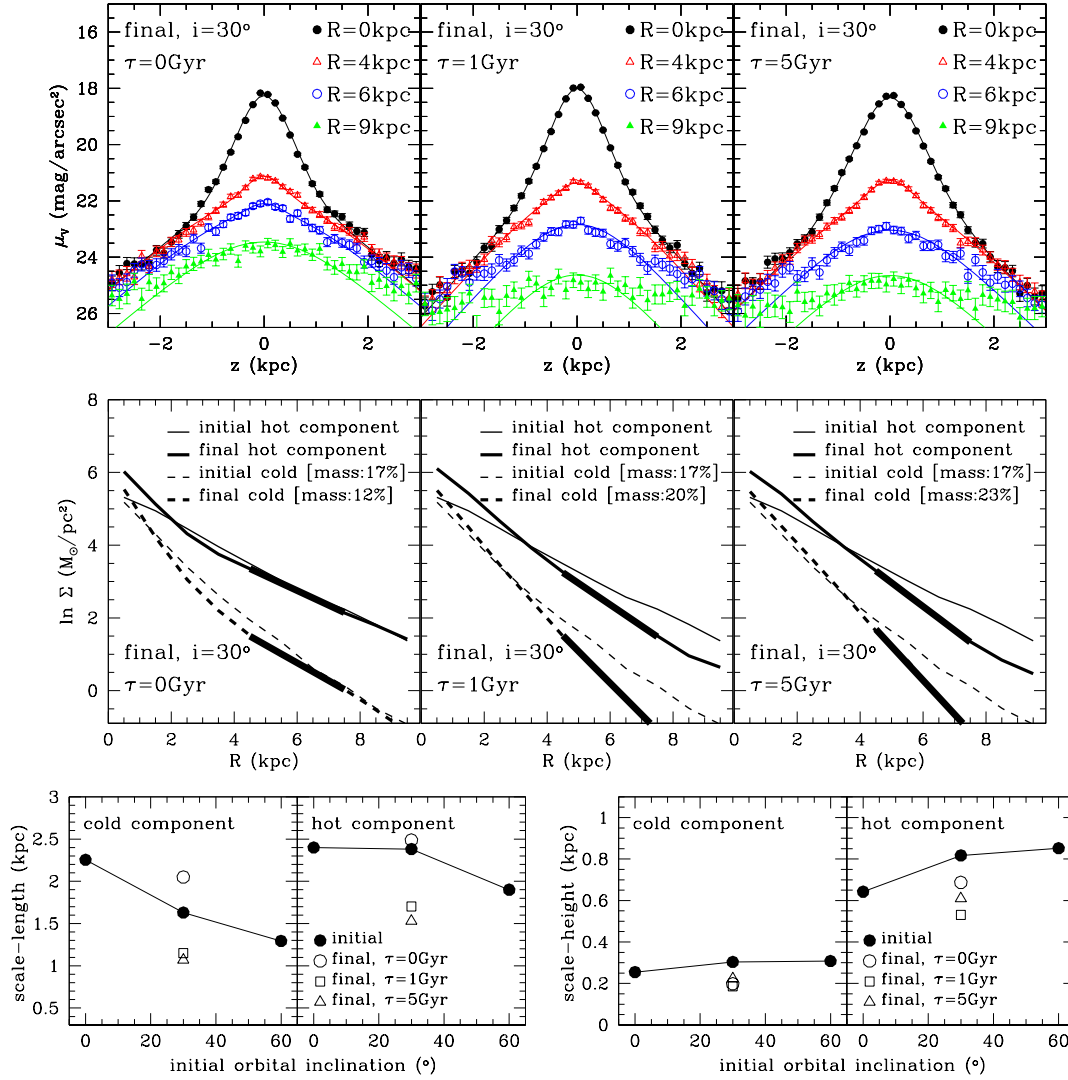


FIG. 6.— Experiment B. Final thick-disk structural properties for different growth timescales of the growing thin disk: $\tau = 0$ Gyr (left panels), $\tau = 1$ Gyr (middle panels), and $\tau = 5$ Gyr (right panels). Rows 1 to 3 are the same as in Figure 5.

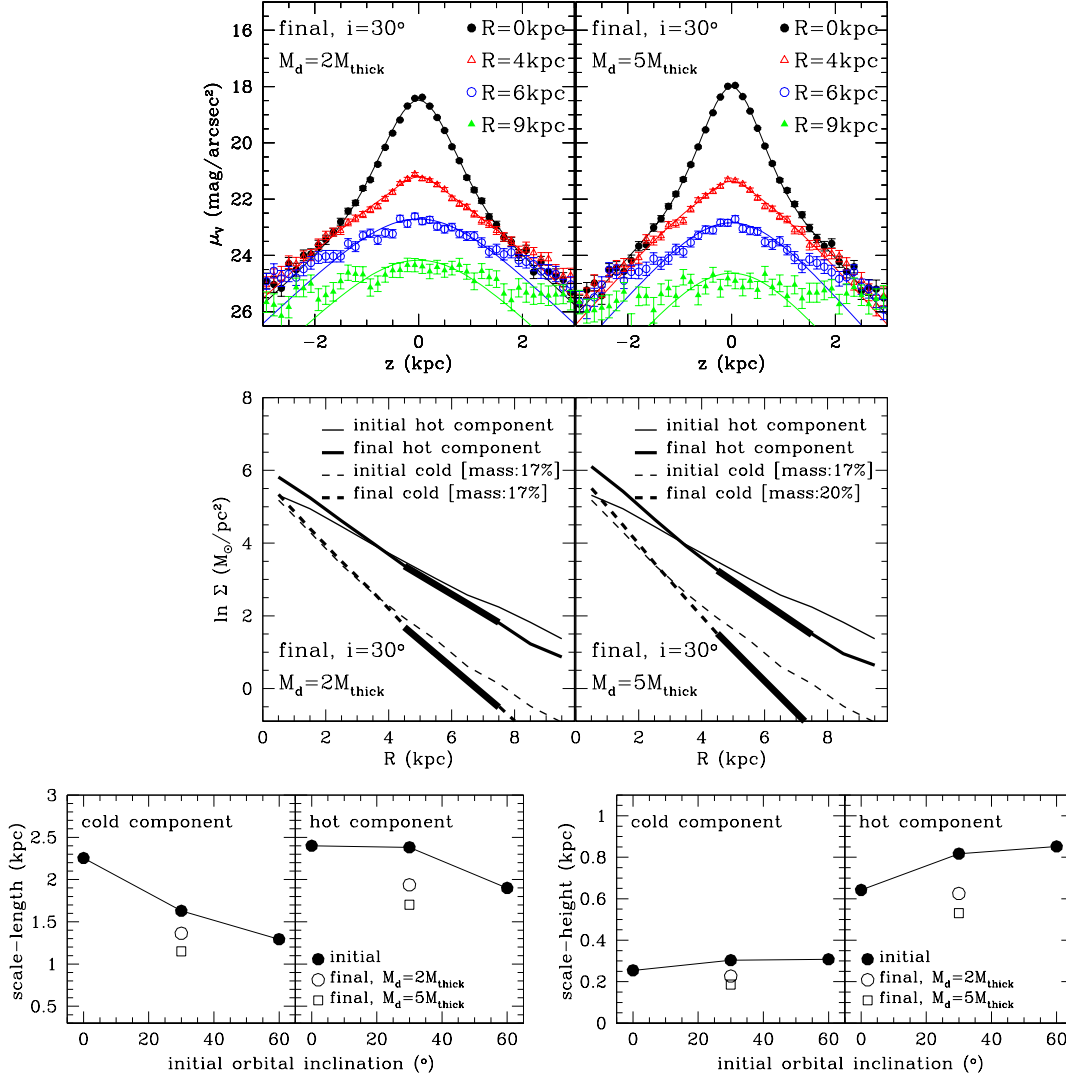


FIG. 7.— Experiment C1. Final thick-disk structural properties for different masses of the growing thin disk: $M_d = 2M_{\text{thick}}$ (left panels) and $M_d = 5M_{\text{thick}}$ (right panels). Rows 1 to 3 are the same as in Figure 5.

evolution does not have a strong dependence on the growth timescale of the new thin disk for $\tau=1$ and 5 Gyr. In both cases, the peak of the final vertical surface brightness profiles becomes narrower and is characterized by a central value that is ~ 1 magnitude brighter than that of the initial configuration. However, at distances $R > 4$ kpc, the surface brightness levels near the plane ($z = 0$ kpc) are lower compared to the initial thick disk. Both features reflect the radial and vertical contraction discussed above. Moreover, the initial scale-heights of the cold and hot components decrease by 20–35% after the accretion event. While the scale-lengths have decreased by $\sim 30\%$ for both the cold and hot component, the radial surface density profiles are very similar for both timescales.

On the other hand, the most dramatic feature of the experiment with the instantaneous growth is the “break” at $R \sim 3\text{--}4$ kpc of the originally exponential surface density profiles of both the cold remnant and the hot/thicker component. For $\tau = 0$ Gyr the central surface densities reach similar values to those of the $\tau = 1$ Gyr and $\tau = 5$ Gyr cases, while in the region $R > 4$ kpc they show little evolution compared to the initial system.

Experiment C1 shows that a factor of 2.5 more massive growing thin disk causes roughly twice more contraction in the initial thick disk in terms of scale-length and scale-height. Interestingly, the mass fraction associated with the cold component of the thick disk increases by only $\sim 3\%$ (this equivalent to a mass increase in the cold component of roughly 10%) (Figure 7). On the other hand, the thickness of the growing thin disk (experiment C2) does not seem to impact significantly the structural evolution of the thick disks, as shown in Figure 8, where the left and right panels correspond to $z_d = 25$ pc and $z_d = 125$ pc, respectively. For example, in both cases the scale-lengths decreased by $\sim 30\%$, while the scale-heights decreased by $\sim 40\%$. Finally, variations in the scale-length of the new disk (experiment C3) lead to a change in the mass fraction associated with the cold component of the thick disk. Thin disks with a scale-length 3 times smaller (Figure 9) reduce the mass of the cold remnant to one third. This can be expected since a growing disk with a larger radial extent would be able to attract more mass onto the midplane across the system. No significant differences are detected in the final scale-lengths and scale-heights of both components

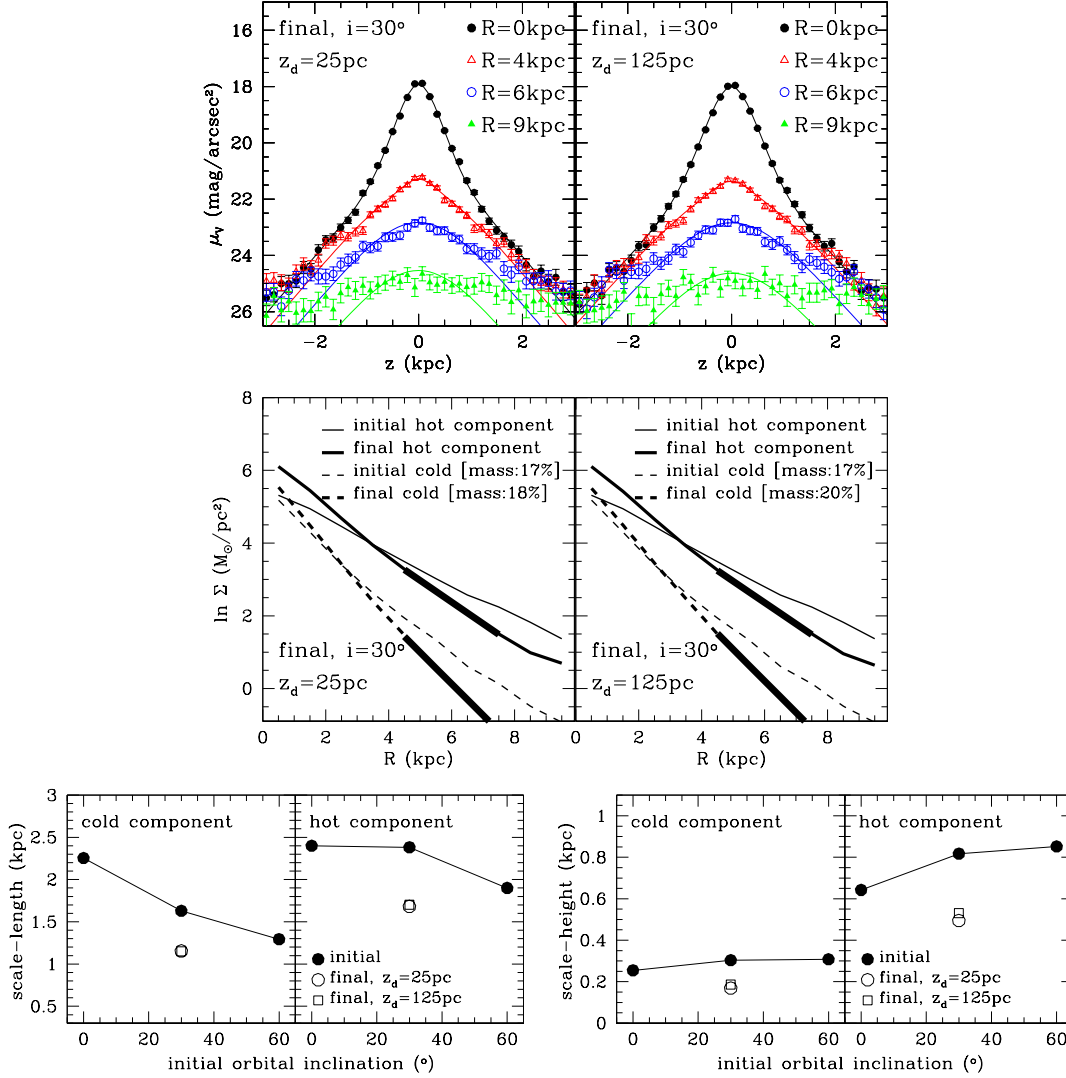


FIG. 8.— Experiment C2. Final thick-disk structural properties for different vertical scale-heights of the growing thin disk: $z_d = 25$ pc (left panels) and $z_d = 125$ pc (right panels). Rows 1 to 3 as in Figure 5.

in the contracted thick disks. However, the estimation of the final scale-length of the cold remnant in the case of a new disk with $R_d = 1$ kpc should be taken with caution, since it could be affected by the “break” feature of the surface density and by the region chosen to derive the scale-length.

We remind the reader that the previous analysis does not include stars from the growing thin disks. Therefore, it is important to clarify the extend to which the structural decomposition of the final thick disks depends on the inclusion of the growing thin disks. Such an attempt is presented in Figure 9 which compares the final thick-disk vertical surface brightness profiles in experiment C3 ($R_d = 1$ kpc) with and without the inclusion of the growing thin disk. Not unexpectedly, when the growing thin disk is included in the decomposition, the peak of the surface brightness profiles increases at all radii. However, the scale-heights of both “cold” and “hot” components are not substantially modified. Specifically, when the growing thin disk is included, scale-heights change from 140 pc and 585 pc to 130 pc and 650 pc. We find a similar behavior in the rest of our experiments for the scale-heights. It is important to note that other properties can

be affected more by the inclusion of the growing thin disk in the analysis (e.g., scale-lengths). However, the magnitude of these differences depends sensitively on the criteria that are used to define the regions dominated by the “cold” and “hot” component, that is $|z| < 0.5z_{\text{cold}}$ and $z_{\text{cold}} < |z| < 3$ kpc, respectively, in terms of the scale-height of the “cold” component (see Paper I).

In the numerical simulations discussed in Paper I, the angular momenta of the dark matter halos and thick disks were often slightly misaligned by few degrees⁷. In experiment D, we utilized the thick disk produced by an accretion event with an initial inclination of $i = 30^\circ$. The angular momentum vector of the adopted thick disk is misaligned by $\sim 6^\circ$ with respect to the halo angular momentum. For this experiment we have allowed the angular momentum of the growing thin disk to be aligned with the angular momentum of either the halo or

⁷ Cosmological simulations show that the angular momentum of the baryonic component of a galaxy correlates well with the angular momentum of the parent dark matter halos, with a typical misalignment of $\sim 20^\circ$ (Sharma & Steinmetz 2005).

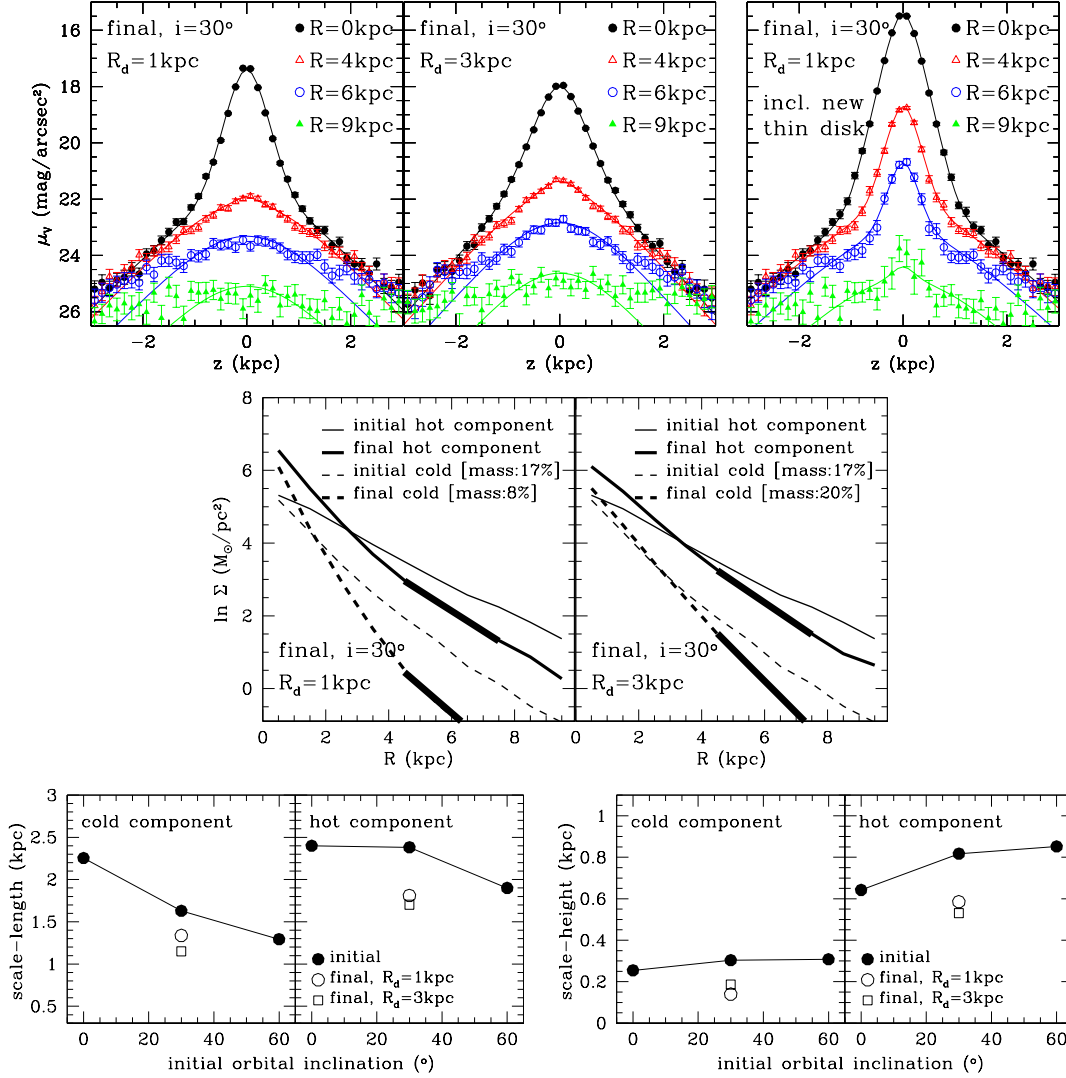


FIG. 9.— Experiment C3. Final thick-disk structural properties for different radial scale-lengths of the growing thin disk: $R_d = 1$ kpc (left panels) and $R_d = 3$ kpc (right panels). Rows 1 to 3 as in Figure 5. The top right panel shows the results when the growing thin disk is included in the decomposition analysis.

the thick disk. Figure 10 shows that no significant differences can be detected in the structure of the thick disks for either alignment of the growing disk, which is not surprising given the rather small misalignment between the initial thick disk and the halo angular momenta. In principle, the differences in the evolution of the properties of the thick disk could become larger for a more significant initial misalignment.

In experiment E (Figure 11) the adopted initial thick disks have been produced by an accretion event with an initial inclination of $i = 0^\circ$. We considered two cases where the infalling satellite was on a prograde and on a retrograde orbit with respect to the rotation of the pre-existing galactic disk. In both cases, a significant amount of angular momentum is transferred from the satellite to the dark matter halo (see Vitvitska et al. 2002; Hetzner & Burkert 2006) and much less into the pre-existing disk. The latter is because by the time the satellite has reached the disk the orbit is much smaller than the initial one, and it has lost most of its bound mass. As a result, the halo and the resulting thick disk rotate in the same sense after the accretion event in the prograde case, while in the retrograde case they rotate in opposite directions. We note

that our initial dark matter halos are non-rotating, but the same conclusions would hold for halos with typical amounts of initial rotation (see below).

The surface density profiles in Figure 11 show that the growth of a thin disk on thick disks with opposite sense of rotation induces essentially the same increase in the mass fraction associated with the thin remnant (from $\sim 15\%$ initially to $\sim 22\%$), and that the decrease in the scale-length of the thin remnant is of similar amplitude ($\sim 30\%$). The most significant difference seems to be in the scale-lengths of the thick disk, where in the prograde case it is induced a decrease of 25%, while in the retrograde one it is induced only a 7% decrease (as for experiment C3 this has some dependency on the region considered to estimate the scale-lengths). On the other hand, the evolution of the scale-heights of both the thin remnant and the thick disk do not show a significant difference between prograde and retrograde cases.

This experiment was motivated by recent observations of counter-rotating thick disks (with respect to their thin disks) detected by Yoachim & Dalcanton (2005). It has been suggested that such counter-rotation may pose difficulties for the

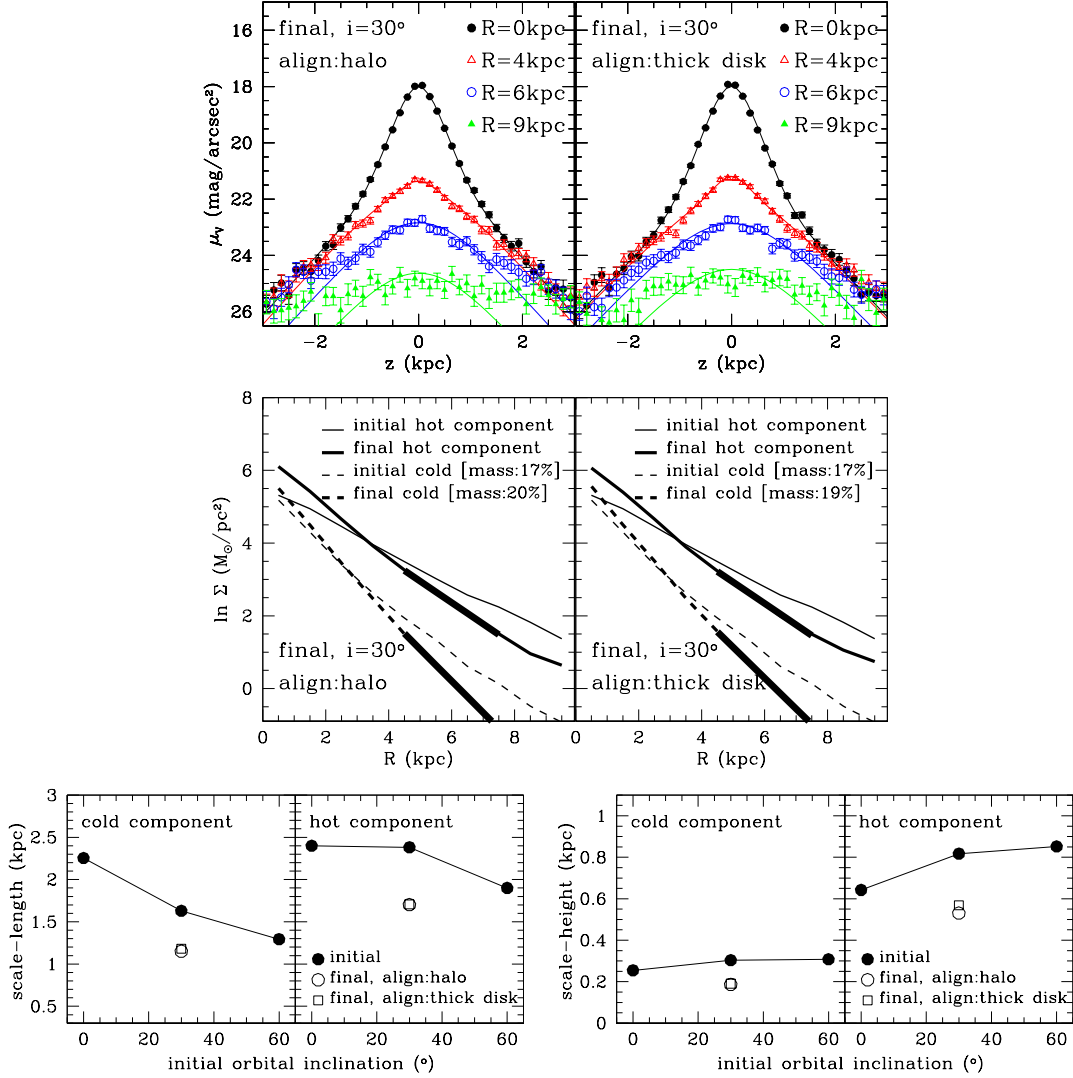


FIG. 10.— Experiment D. Final thick-disk structural properties for different alignments of the total angular momentum vector of the growing thin disk: either along the angular momentum of the dark matter halo (left panels) or along the angular momentum vector of the thick disk (right panels). Rows 1 to 3 as in Figure 5.

disk heating scenario as a viable model for the formation of thick disks. However, an encounter between a pre-existing thin disk galaxy and a massive satellite on a retrograde orbit can, in principle, produce a thick disk and a counter-rotating dark matter halo. In order to illustrate this we can estimate the total angular momentum of a halo after such encounter as $L_i^{\text{halo}} = L_i^{\text{halo}} + L_i^{\text{sat}}$, where the last term on the right is the initial orbital angular momentum of the infalling satellite. L_i^{halo} can be computed using the halo spin parameter, λ , and its virial properties as $L_i^{\text{halo}} = \sqrt{2}\lambda M_{\text{vir}} V_{\text{vir}} R_{\text{vir}}$ (Bullock et al. 2001). On the other hand, $L_i^{\text{sat}} = M_{\text{sat}} R_0 V_0$, in terms of the satellite mass and its initial orbital radius and velocity. In the case of experiment E2, $M_{\text{vir}} = 5.07 \times 10^{11} M_{\odot}$, $V_{\text{vir}} = 133.87 \text{ km s}^{-1}$, $R_{\text{vir}} = 122.22 \text{ kpc}$, $M_{\text{sat}} = 10^{11} M_{\odot}$, $R_0 = 83.9 \text{ kpc}$, and $V_0 = -78.8 \text{ km s}^{-1}$ (negative sign indicates a retrograde orbit). Thus, assuming a typical value for the spin parameter, $\lambda = 0.035$, we have $L_i^{\text{halo}} = -2.5 \times 10^{14} M_{\odot} \text{ kpc km s}^{-1}$, where the negative sign shows that the halo is counter-rotating with respect to its initial state.

Freshly accreted cold gas from the galactic halo would have its angular momentum aligned with that of the dark halo and therefore could form a young thin disk that is counter-rotating with respect to the older thick disk. In this case, the new disk would also counter-rotate with respect to any old thin remnant present.

3.2. Kinematical Evolution of Thick Disks

3.2.1. General Features

Similarly to the structural evolution, the growth of a thin disk induces two characteristic changes in thick-disk kinematics that are common to all experiments. In particular, a growing thin disk causes an increase in both the mean rotational velocity and the velocity dispersions of the thick disks. Both effects can be explained by the fact that the growing thin disk adds mass to the system and by the subsequent structural contraction described above.

3.2.2. Experiments from A to E

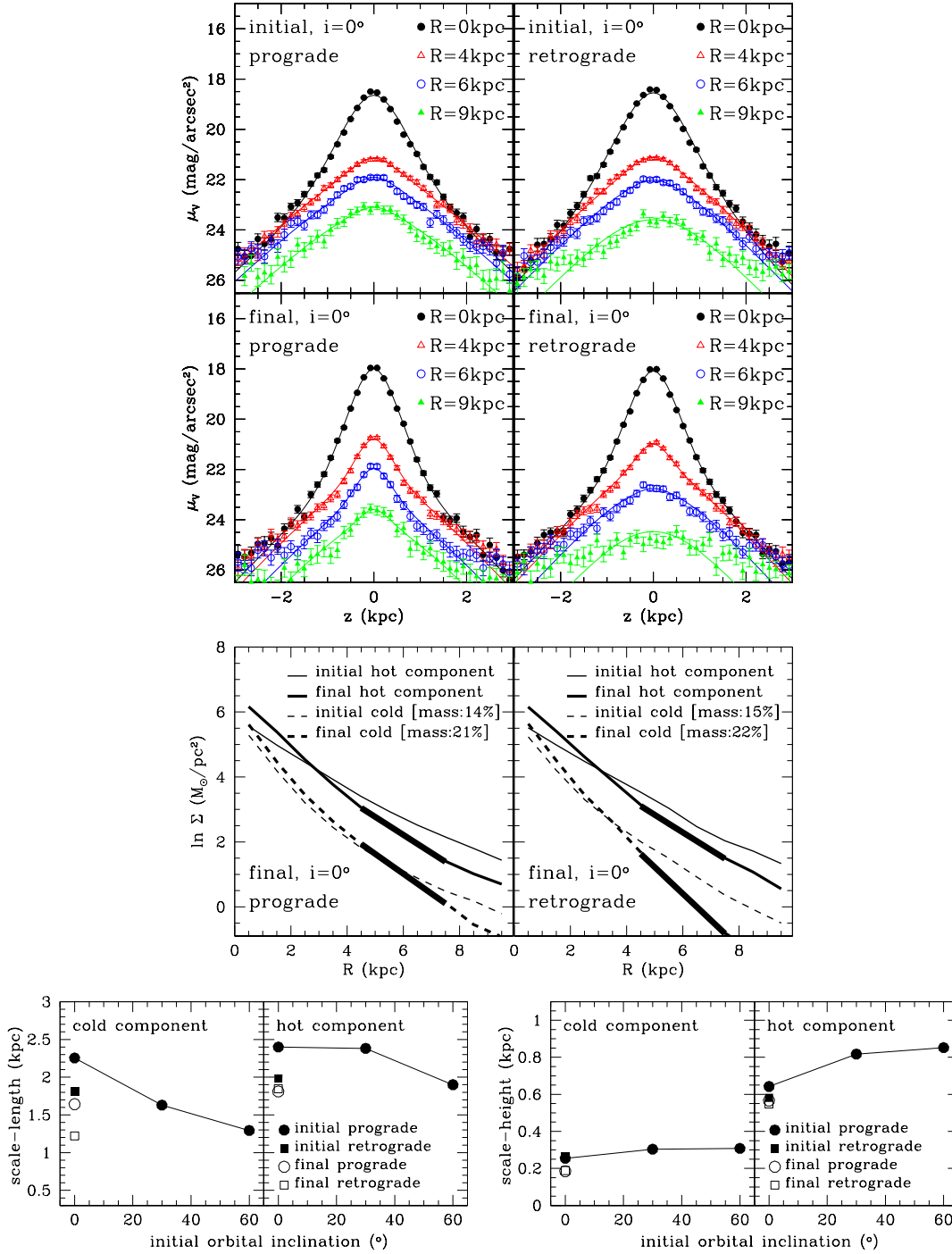


FIG. 11.— Experiment E. Final thick-disk structural properties for different sense of rotation of the initial thick disk: prograde (left panels) and retrograde (right panels). Rows 1 to 3 as in Figure 5.

Figure 12 presents the initial and final global kinematics of the simulated thick disks as a function of galactocentric radius. We characterize the thick-disk kinematical response to the growth of a new thin disk through the evolution of the mean rotational velocity, $\langle V_\phi \rangle$, and velocity ellipsoid $(\sigma_R, \sigma_\phi, \sigma_z)$, where σ_R , σ_ϕ , and σ_z correspond to the radial, azimuthal, and vertical velocity dispersions, respectively. These properties are computed within $R < 10$ kpc and $|z| < 4$ kpc and as before no stars from the growing thin disks have been

included in the analysis. It is important to mention that we do not find significant differences between the kinematics of the global thick disks (i.e. “cold” + “hot” components) and those from the “hot” component alone in the case of σ_R and σ_ϕ . However, σ_z and V_ϕ of the “hot” component are larger, as expected, by $\sim 20 \text{ km s}^{-1}$ and $\sim 40 \text{ km s}^{-1}$, respectively (mainly at smaller radii).

The results of experiment A demonstrate that after the growth of the new thin disk, the velocity dispersions of the

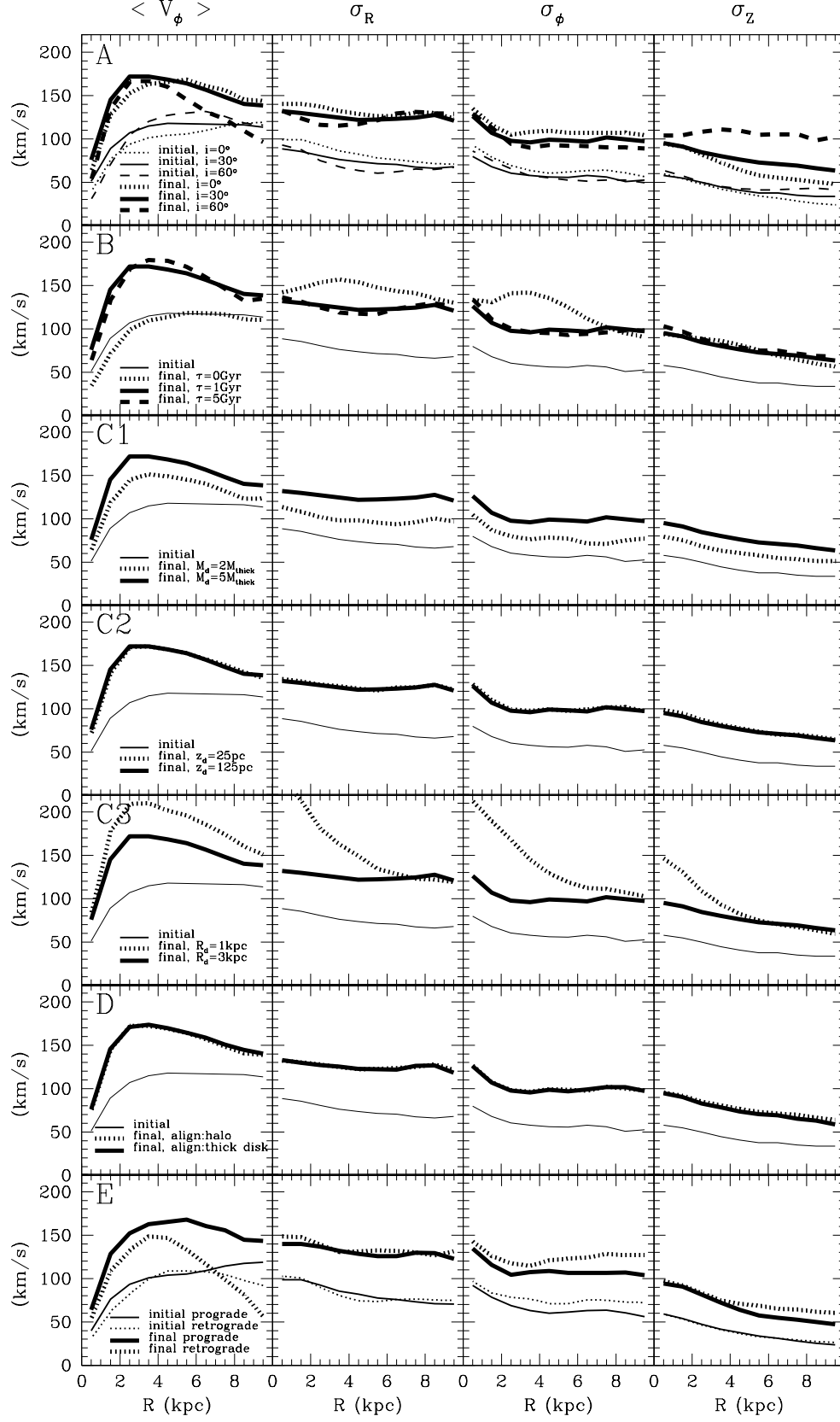


FIG. 12.— Thick-disk kinematical properties in experiments from A to E. Results are shown for both initial and final thick disks.

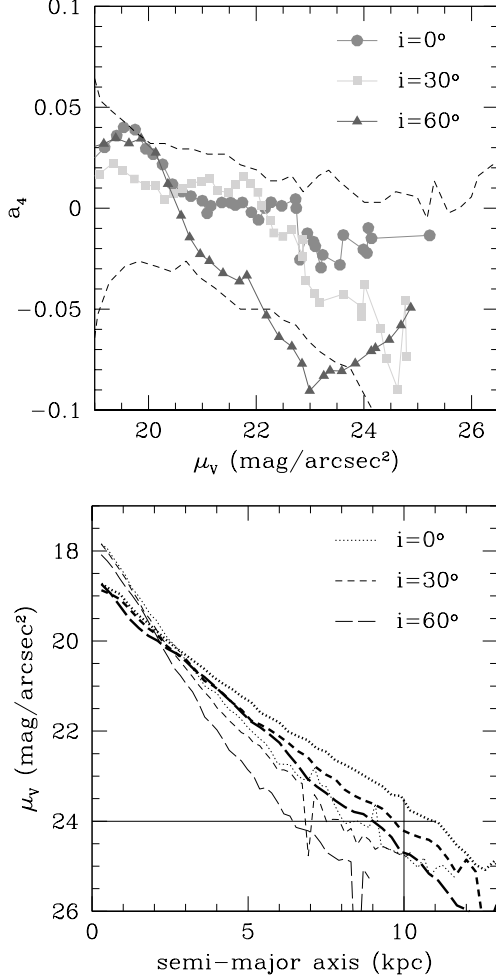


FIG. 13.— *Upper panel:* a_4 isophotal shape parameter as a function of isophotal surface brightness in the V-band for the final thick disks in experiment A. Dashed curves show results before the growth of the new disk (see Figure 8 of Paper I) and are included here as a reference. *Bottom panel:* V-band surface brightness as a function of the isophotal semi-major axis for the same experiment. Thick and thin lines show the profiles before and after the thin-disk growth, respectively. The solid horizontal line marks the surface brightness limit below which the isophotes are consistently boxy. The vertical solid line marks the limiting radius R within which the global properties of the final thick disks are computed.

final thick disks maintain the original trends with the satellite orbital inclination (that is, the hotter the initial thick disk the hotter the final one). We note that the mean rotational velocity in the 60° case shows a clear decrease at larger radii which is due to the increasing skewness of the total V_ϕ distribution towards lower velocities. This is a consequence of the contribution of the accreted stars, which are preferentially found in the outskirts and which rotate more slowly with respect to the stars of the pre-existing thin disk.

The findings of experiment B indicate that for $\tau=1$ and 5 Gyr the global kinematics of the final thick disks do not depend on the growth timescale of the new disk. Interestingly, the effect of the instantaneous growth is more complex. In this case, the mean rotation of the thick disk is not substantially affected by the growth of the new disk (except by some decrease in the inner region). This is consistent with the corresponding surface density profile (Figure 6) which shows little variation with respect to the initial configuration (except by a distinc-

tive “break” at $R \sim 4$ kpc). Although a significant amount of mass has been added to the system via the growth of the new thin disk, this growth was strongly non-adiabatic. This fact implies that the eccentricity of the stellar orbits in the thick disk must have changed significantly, or equivalently, that the amount of ordered (circular) motion must be much smaller. Thus in practice, the extra potential energy due to the new thin disk must have gone into random motions in the plane as can be seen from the central panels in Figure 12, which clearly show an increase in the velocity dispersions, particularly at $R \sim 4$ kpc.

The results of experiment C1 show that a more massive growing disk induces a larger increase in both the mean rotation and the velocity dispersions of the final thick disks. By resorting to the Jeans equations (Binney & Tremaine 1987, Eq. 4.29), it may be expected that a thin disk roughly twice as massive causes an increase of a factor of 2 in all thick-disk velocity dispersions and in the mean rotational velocity at a given radius.

The findings of experiment C2 suggest that for our choices of vertical scale-heights, $z_d = 25$ and 125 pc, the kinematical evolution of thick-disk stars does not depend essentially on the thickness of the growing disk. Of course, this conclusion is valid as long as the mass of the growing disk is the same as in our case. On the other hand, the results of experiment C3 highlight that at a fixed mass a more radially compact growing disk is responsible for generating a larger increase in both the mean rotational velocity and velocity ellipsoid in the inner regions of thick disks.

The results of experiment D show that the relative alignment of the new disk (with respect to either the halo or the initial thick disk angular momentum) does not seem to affect the kinematical evolution of thick disks. This could also have been expected from the lack of structural evolution shown in Figure 10. Note, however, that the misalignment between the halo and initial thick disk angular momenta is only $\sim 6^\circ$. Such misalignment may be possibly too small to induce significant differences in both the structure and kinematics of the final thick disks.

The findings of experiment E demonstrate that the evolution of all three velocity dispersions is very similar for both prograde and retrograde thick disks, as expected from Figure 11. Note that for the retrograde case there is a significant decrease in the mean rotation of the thick disk at $R > 4$ kpc. Similarly to experiment A2, a closer inspection shows that there is significant skewness in the distribution of V_ϕ towards lower velocities. This is due to the contribution of satellite stars at large radii which rotate more slowly than disk stars. Overall, in the retrograde case the evolution in the kinematics of the thick disk is found to be very similar to that in the prograde case. The most significant difference is found in σ_z where the retrograde case leads to a somewhat higher dispersion at large radii.

4. COMPARISON WITH INITIAL THICK DISKS

4.1. Structure

The results presented in Figure 8 of Paper I show that the outer isophotes of the simulated thick disks measured at surface brightness $\mu_V > 25$ mag arcsec⁻², namely > 6 mag below the central peak $\mu_V \sim 19$ mag arcsec⁻², are consistently more boxy than the inner ones. This characteristic feature is present in all the thick disks simulated in Paper I, implying that the detection of such a degree of boxiness in real galaxies

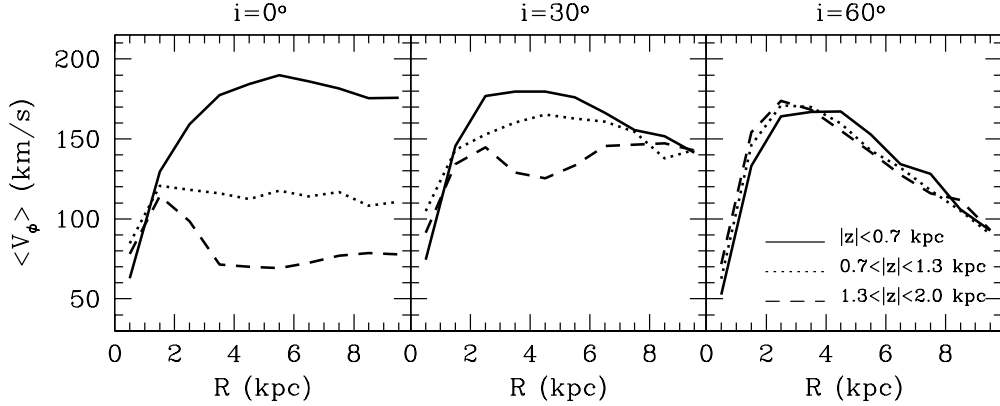


FIG. 14.— Final mean azimuthal velocity of thick-disk stars as a function of galactocentric distance, R . Results are presented for experiment A at various scale-heights above the disk plane. The vertical gradient of the mean azimuthal velocity depends sensitively on the orbital inclination of the infalling satellite that produced the initial thick disks.

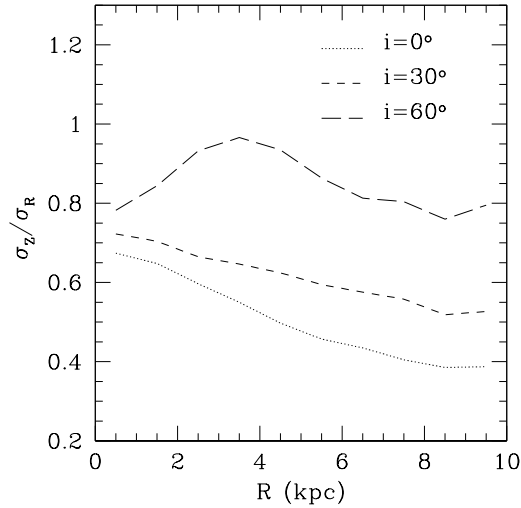


FIG. 15.— Final velocity dispersion ratio σ_z/σ_R of thick-disk stars as a function of galactocentric distance, R . Results are shown for experiment A. Even after the growth of the new thin disk, the velocity dispersion ratio σ_z/σ_R depends sensitively on the orbital inclination of the infalling satellite.

could be used to test thick-disk formation scenarios (see also Bournaud et al. 2009).

Figure 13 shows the a_4 parameter as a function of isophotal surface brightness in the V-band for the final thick disks of experiment A. This figure shows that the trend of more boxy contours at lower surface brightness limits is maintained after the growth of the new disk. Interestingly, at a given μ_V , the contours are slightly less boxy in comparison to those presented in Figure 8 of Paper I. This is likely caused by the growth of the new (flatter and more massive) thin disk. Recall that Figure 1 shows that contours at lower μ_V are in general closer to the center of the system after the induced structural contraction. In order to detect the “boxiness” in the experiments with growing disks one would need to reach surface brightness levels beyond $\mu_V > 24\text{--}25\text{ mag arcsec}^{-2}$, namely $> 6\text{--}7\text{ mag}$ below the central peak of the thick disks after the growth of the new disk, $\mu_V \sim 18\text{ mag arcsec}^{-2}$.

The bottom panel of Figure 13 shows for the same experiment the isophotal surface brightness as a function of the isophotal semi-major axis before and after the growth of the

new disk. The results in this panel suggest that a possible cause for the structural change introduced to the vertical surface brightness profiles in the outskirts of the final thick disks (see Figure 4) is the contraction which brings boxy isophotes within the region $R < 10\text{ kpc}$. To this end, the presence of boxy contours at the outskirts would enhance the separation between inner contours (that are more packed together) and outer contours (see Figure 1). This would make more noticeable the difference in the profile shown in Figure 4 (right) between $|z| < 1\text{ kpc}$ and $|z| > 2\text{ kpc}$.

The structure of the initial thick disks is in good agreement with observations of external galaxies and the MW in terms of thick-to-thin ratios of both scale-lengths and scale-heights (see Section 4.2 of Paper I). This conclusion was based on the assumption that thick-disk structure would *not* be strongly affected by the growth of a new thin disk *and* that this thin disk would follow the same distribution as the cold component of the thick disk. Overall, the results of the present paper indicate that thick disks *do* respond to the growth of an embedded thin disk. It is interesting to investigate how these scale ratios compare to observations after the formation of the new thin disk. In our new experiments, we find the final thick-to-thin scale-height ratio to be $\sim 0.6/0.125 = 4.8$, which is still within the range 2.4–5.3 observed in the MW and in S0 galaxies (see Buser et al. 1999; Pohlen et al. 2004; Yoachim & Dalcanton 2006).

In what follows we assume that the Galactic thick disk originated from the vertical dynamical heating of a primordial thin disk by infalling satellites (Kazantzidis et al. 2008; Paper I). It is interesting to use the results above and attempt to determine the initial properties of the initial thick disk of the MW, namely those before the structural contraction induced by the formation of the current thin disk; as well as the properties of the pre-existing disk, namely those before the interaction with the satellite. For example, we typically find that the scale-length of the thick disk after the encounter with the satellite increases by a factor $f_{\text{merger}}^R \sim 1.3\text{--}1.45$, as shown in Section 3.4 of Paper I. On the other hand, the formation of a factor of 5 more massive thin-disk component leads to a decrease in the scale-length of $f_{\text{contr}}^R \sim 0.6$. This implies that the scale-length of the pre-existing disk is given by $R_d^{\text{initial}} = (f_{\text{merger}}^R \times f_{\text{contr}}^R)^{-1} \times R_{d,\text{thick}}^8$ or $R_d^{\text{initial}} \sim$

⁸ Of course, such a relation is only valid under the assumption that the only

$1.15R_{d,\text{thick}}$, which is comparable to the present-day value of the thick disk. This suggests that the radial expansion caused by the accretion event is nearly completely balanced by the contraction induced by the growth of the thin disk. Moreover, using current estimates for the thick-disk scale-length of $R_{d,\text{thick}} = 2.5 - 3$ kpc, we deduce the initial scale-length of the Galactic pre-existing disk to be $R_d^{\text{initial}} \sim 2.9 - 3.5$ kpc. Of course, this could represent a considerable problem, since disks are expected to have been (significantly) smaller in the past (Buitrago et al. 2008).

Similarly, we may compute the initial scale-height of the thick disk of the MW from $f_{\text{merger}}^z \sim 4.7$ and $f_{\text{contr}}^z \sim 0.6$ (both for a 30° inclination encounter). Thus, after assuming for the current thick disk a value of $z_{d,\text{thick}} = 1$ kpc, we compute the scale-height of the pre-existing disk as $z_d^{\text{initial}} \sim 340$ pc. Therefore, we estimate the vertical structure of the pre-existing disk to be similar to that of the current Galactic thin disk.

Especially relevant in this context is the study of Elmegreen & Elmegreen (2006) who investigated thick disks in the Hubble Space Telescope Ultra Deep Field (UDF). These authors examined whether the process of adiabatic thick-disk contraction could have determined the present-day scale height of the thick disk of the MW whose midplane density ratio of thick-to-thin disk is 12% (e.g., Jurić et al. 2008). Their calculations showed that if the present thick-disk component of the MW (with an estimated exponential scale-height of 875 pc) began as an equilibrium pure-thick disk at a young age, and if subsequent accretion of the entire thin disk was adiabatic, then the initial thick-disk sech^2 scale-height had to be ~ 3 kpc (i.e. exponential scale-height ~ 1.5 kpc). Such a value is considerably larger than that observed for young thick disks in the UDF, where the average scale height is 1.0 ± 0.4 kpc. We note that the magnitude of the contraction induced in the thick disk by the growth of the new thin disk reported by Elmegreen & Elmegreen (2006), $f_{\text{contr}}^z \sim 0.6$, agrees well with our estimates.

4.2. Kinematics

Paper I showed that when the thick disks are not decomposed into cold and hot components, their mean rotational velocities exhibit clear gradients as a function of height (see their Figure 20). The magnitude of these vertical gradients depends sensitively on the initial satellite orbital inclination, with larger gradients corresponding to lower inclinations.

Figure 14 shows the variations in the mean rotational velocity of the final thick disks in experiment A as a function of galactocentric distance. Interestingly, after the growth of the new thin disk the vertical gradients are retained, maintaining their dependence on satellite orbital inclination. As concluded in Paper I, the possible detection of such vertical gradients in the thick disk of the MW (e.g. Girard et al. 2006; Ivezić et al. 2008) would suggest a satellite accretion event with a low or intermediate inclination, if the Galactic thick disk was formed via the dynamical heating of a preexisting thin disk. Note also the progressive decrease of the mean rotation at outer radii for larger inclinations. As we illustrate below, this is due to the fact that stars from the heated disk and those from the satellite have rather different z -components of angular momentum at those radii (see Figure 16).

relevant processes are the satellite accretion event and the thin-disk growth, and that secular evolution processes are unimportant in establishing the galactic structure.

Paper I also demonstrated that the velocity dispersion ratio σ_z/σ_R is a fairly accurate discriminator of the initial orbital inclination of the accreted satellite (see their Figure 21). Recent observations in the solar neighborhood report $\sigma_z/\sigma_R \sim 0.6$ (e.g. see Layden et al. 1996; Chiba & Beers 2001; Soubiran et al. 2003; Alcobé & Cubarsi 2005; Vallenari et al. 2006). Assuming that the Galactic thick disk was formed according to the disk heating scenario, such a value may be suggestive of an encounter with a satellite on a low/intermediate orbital inclination (Paper I). Figure 15 shows the final thick-disk dispersion ratio σ_z/σ_R as a function of galactocentric distance in experiment A. It is interesting that the conclusions previously drawn are still valid after the growth of the new thin disk. An interaction with a satellite on a low/intermediate initial inclination is still required to obtain a value of $\sigma_z/\sigma_R \sim 0.6$. We note that similar results are valid for the rest of the experiments presented in this study.

For the experiment with initial inclination 30° , we find that after the satellite accretion event the thick-disk velocity dispersions increase by factors $(f_R, f_\phi, f_z)_{\text{merger}} \sim (2, 1.7, 1.5)$. These values are obtained by measuring the velocity dispersions at $2.4R_d$ and at $2.4R_{d,\text{thick}}$ (see Table 1 and Figure 14 of Paper I, for “ $z=1$ ”). Additionally, the growth of a factor of 5 more massive new disk further increases the velocity dispersions by factors $(f_R, f_\phi, f_z)_{\text{contr}} \sim (1.8, 2, 2.2)$, where the final velocity dispersions were measured at $2.4R_{d,\text{thick}}^{\text{final}}$ (see bottom panel of Figure 6). As in the case of computing the scale-height of the pre-existing disk, we can estimate its initial velocity dispersions as $(\sigma_R^{\text{initial}}, \sigma_\phi^{\text{initial}}, \sigma_z^{\text{initial}}) \sim (18, 16, 12) \text{ km s}^{-1}$. This calculation assumes observed values for the Galactic thick disk $(65, 54, 38) \text{ km s}^{-1}$ (Layden et al. 1996; Chiba & Beers 2001; Soubiran et al. 2003; Alcobé & Cubarsi 2005; Vallenari et al. 2006; Veltz et al. 2008). The entire process of heating and subsequent contraction leads to an increase by a factor of ~ 3.4 in all velocity dispersions for this particular example.

4.3. Phase-Space

Villalobos & Helmi (2009, hereafter Paper II) showed that the distribution of the z -component of the angular momentum $L_z(R)$ is a good discriminator for separating heated disk and satellite stars, especially at large radii (see their Figure 6). Figure 16 shows both the initial and final L_z distributions of disk and satellite stars for experiment A. Stars are located within $2 < R < 7$ kpc and $|z| < 1$ kpc. Interestingly, the initial separation between disk and satellite stars is now less clear compared to that in Figure 6 of Paper II. This is likely due to differences in the intrinsic kinematics of the satellites used in each case (spherical versus disk). After the growth of the new disk two effects are expected regarding the L_z distributions of stars. First, disk stars are expected to have a steeper slope in their trend of $L_z(R)$, while satellite stars should roughly maintain their almost flat slope. This is a consequence of both the radial contraction experienced by thick disks and the adiabatic invariance of L_z of each star. Second, both type of stars are expected to have a larger $L_z (= RV_\phi)$ dispersion at a given radius R . This is because of the increase in the V_ϕ velocity dispersion measured after the growth of the new disk (Section 3.2). Both effects can be observed in the left panels of Figure 16. As the slope of disk stars gets steeper, it is expected that the separation between disk and satellite stars would become more noticeable. However, the significant increase in the velocity dispersion appears as the

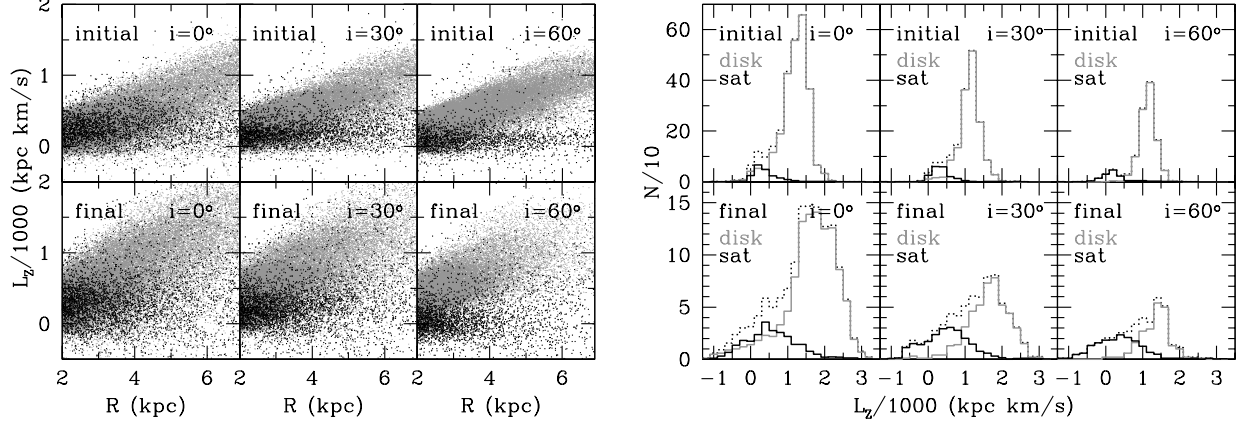


FIG. 16.— *Left panels:* Initial and final scatter plots of vertical angular momentum, L_z , versus galactocentric distance, R , for disk (grey points) and satellite stars (black points). Results are presented for experiment A and for stars that were initially located within $2 < R < 7$ kpc and $|z| < 1$ kpc. For clarity, only one every five stars is plotted. *Right panels:* Initial and final L_z histograms for disk and satellite stars that were initially located within $8 < R < 9$ kpc and $|z| < 1$ kpc. Results are presented for experiment A and dotted lines show the total distributions.

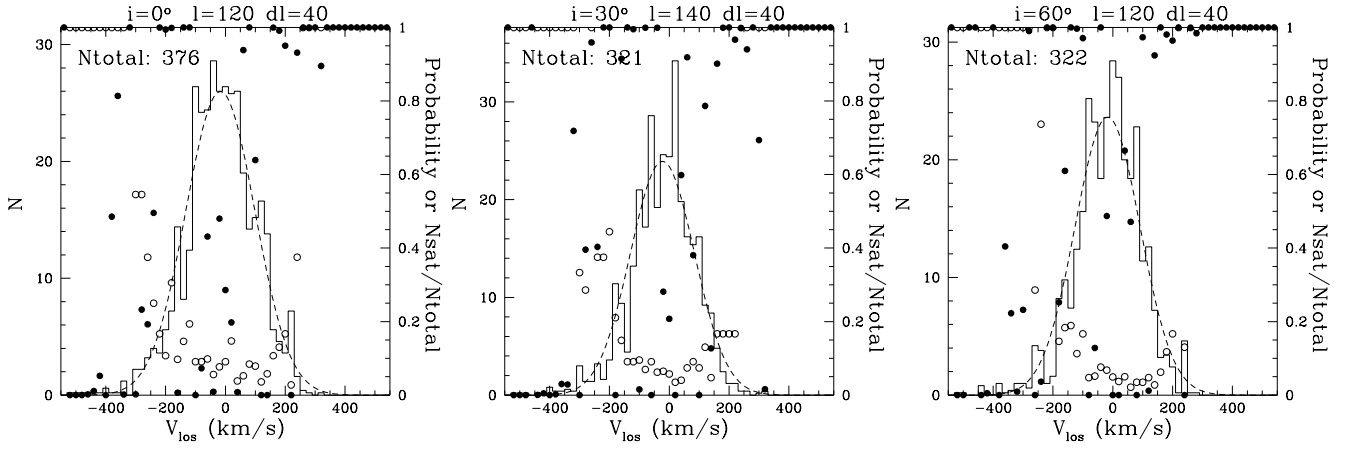


FIG. 17.— Histograms of final heliocentric line-of-sight velocities for thick-disk stars after subtracting the mean rotation of the final thick disks. Results are presented for experiment A and histograms include disk and satellite stars within a slice around $l \sim 140^\circ$, where the contribution of satellite stars to the wings is maximal. The width of l -slices is 40° . Dashed lines present the best-fit Gaussian distributions to the histograms. Open points show the fraction of satellite stars in each velocity bin, while filled points denote the probability of the observed number of stars compared to what is expected from the best-fit Gaussian in each velocity bin.

dominant effect, making the separation even less evident than before the growth of the new disk.

The right panels of Figure 16 present the distributions of disk and satellite stars that were initially located in the solar neighborhood ($8 < R < 9$ kpc) and within $|z| < 1$ kpc. The histograms show that while there is no clear distinction between disk and satellite stars, something that can also be seen in the initial thick disks (except in the 60° case), it is possible to identify a large contribution of satellite stars in the wings of the distributions at low L_z . This causes significant asymmetries in the total distributions. Nevertheless, it is important to note that the trend in L_z of disk stars as a function of R is maintained and thus should be observable in the Galactic thick disk if it was formed via the heating of a pre-existing disk.

Paper II also showed that the wings of the distributions of heliocentric line-of-sight velocities, v_{los} , measured in small volumes in the final thick disks, contain mostly satellite stars. These velocity distributions were found to differ significantly from Gaussians because of the more heavily populated wings

(see Figure 10 of Paper II). Figure 17 shows a very similar behavior for the final thick disks of experiment A. In this case, the volumes are located somewhat closer to the center, at ~ 3 kpc (1.5 kpc radius) to take into account the radial contraction of the systems after the growth of the new disk. However, we remind the reader that the results were not found to depend on either the size or the location of the volumes. It is also important to stress that the dispersions of the v_{los} distributions are significantly larger than those presented in Figure 10 of Paper II. Nonetheless, the same tests used in Paper II to quantify the statistical significance of features present in the v_{los} distributions can successfully detect the contribution of satellite stars to the wings in the present study. These statistical tests measure the likelihood of finding satellite stars at a given velocity bin of a v_{los} distribution by generating a number of random realizations based on the best Gaussian fit to the distribution.

5. SUMMARY AND CONCLUSIONS

Using a suite of collisionless N -body simulations we have examined the evolution of the structural and kinematical prop-

erties of simulated thick disks induced by the growth of an embedded thin disk. Our simulation campaign quantifies the importance of various parameters related to the growing disks that could influence the response of thick disks, including: (1) the growth timescale; (2) the final mass; (3) the vertical scale-height; (4) the radial scale-length; and (5) the sense of rotation of the initial thick disk with respect to its halo (prograde or retrograde).

Our simulations demonstrate that after the growth of the new thin disk, thick-disks experience a strong radial as well as vertical contraction which leads to a significant decrease in their scale-lengths and scale-heights. This contraction is triggered by the deepening of the potential well of the system due to the mass growth associated with the new disk. An important consequence of this contraction is related to the migration of thick-disk stars from the outskirts inwards. Stars that were typically at $R \sim 15$ kpc before the growth of the new disk, are found at $R \sim 9$ kpc after the growth is completed.

Despite the strong contraction, the mass fraction associated with the kinematically cold component of the final thick disks remains $< 25\%$. This is comparable to the mass present in the remnants of the satellite accretion events discussed in Paper I. The outskirts of these disks ($R \sim 3.8 - 5.6 R_{d, \text{thick}}$) present boxy contours at very low surface brightness levels ($> 6 - 7$ mag below the central peak).

We find that the thick-disk structural and kinematical evolution is driven primarily by the total mass and scale-length of the growing thin disk, with a weak dependence on the characteristics of the initial thick disk. Conversely, the thin-disk growth timescale appears to have a minor influence on the final thick-disk structure provided that this timescale is sufficiently long for the process to be considered adiabatic. Similarly, neither the thinness (in terms of scale-height) nor the alignment of its angular momentum vector (either to the halo angular momentum or to that of the thick disk) seem to affect the final properties of the thick disks. The sense of rotation of the initial thick disk has an effect on the radial extension of the cold component of the final thick disk, which is significantly smaller for retrograde rotation.

Kinematically, the growth of a more massive thin disk increases the mean rotation and the velocity ellipsoid of the initial thick disks. The increase in the mean rotation is associated with the larger mass deposited at a given radius after the structural contraction. Moreover, as a consequence of the contraction and additional mass accumulation on the midplane of the

thick disk, the velocity dispersion increase is linked to a significant steepening of the gravitational potential gradient near the disk plane.

We close with a few words of caution and a discussion of fruitful directions for future work that may lead to more conclusive statements about the role of a reforming thin disk in establishing the structural properties of thick disks. We reiterate that we have only modeled the gravitational potential of a thin disk that slowly grows in mass over time in the collisionless regime, and we have neglected both the cosmological context and the complex interplay of effects (e.g., gas cooling, star formation) relevant to the formation and evolution of spiral galaxies. Previous studies have been carried out in the context of galactic mergers including gas physics (Barnes & Hernquist 1996; Kazantzidis et al. 2005; di Matteo et al. 2007; Hopkins et al. 2008; Bournaud et al. 2009; Callegari et al. 2009; Moster et al. 2009) and within a cosmological context (Governato et al. 2007), therefore we consider that an important future study will be to follow self-consistently, as the satellites fall in, the growth of the new thin disk via accretion-induced bursts of star formation, deposition of gas by the accreting satellites themselves, and smooth gas accretion through the cooling of hot gas in the galactic halo. While a full exploration of these contingencies is challenging, we intend to extend the present investigation in this direction in a forthcoming work.

The authors are grateful to the organizers of the Ensenada meeting on “Galaxy Structure and the Structure of Galaxies” for providing the right atmosphere and setting to initiate this project. SK would like to thank Mandeep Gill and David Weinberg for many stimulating discussions. SK is supported by the Center for Cosmology and Astro-Particle Physics (CCAPP) at The Ohio State University. AV and AH acknowledge financial support from the Netherlands Organization for Scientific Research (NWO). This work was supported by an allocation of computing time from the Ohio Supercomputer Center (<http://www.osc.edu>). The numerical simulations performed to produce the thick disks used as initial conditions in this study were conducted in the Linux cluster at the Center for High Performance Computing and Visualization (HPC/V) of the University of Groningen in The Netherlands. This research made use of the NASA Astrophysics Data System.

REFERENCES

- Alcobé, S., & Cubarsi, R. 2005, *A&A*, 442, 929
Ardi, E., Tsuchiya, T., & Burkert, A. 2003, *ApJ*, 596, 204
Bahcall, J. N., & Soneira, R. M. 1980, *ApJS*, 44, 73
Barnes, J., & White, S. D. M. 1984, *MNRAS*, 211, 753
Barnes, J. E., & Hernquist, L. 1996, *ApJ*, 471, 115
Baugh, C. M. 2006, *Reports on Progress in Physics*, 69, 3101
Belokurov, V., et al. 2006, *ApJ*, 642, L137
Benson, A. J. 2005, *MNRAS*, 358, 551
Benson, A. J., Lacey, C. G., Frenk, C. S., Baugh, C. M., & Cole, S. 2004, *MNRAS*, 351, 1215
Binney, J., & Tremaine, S. 1987, *Galactic dynamics* (Princeton, NJ: Princeton University Press, 1987, 755 p.)
Blumenthal, G. R., Faber, S. M., Flores, R., & Primack, J. R. 1986, *ApJ*, 301, 27
Blumenthal, G. R., Faber, S. M., Primack, J. R., & Rees, M. J. 1984, *Nature*, 311, 517
Bournaud, F., Elmegreen, B. G., & Martig, M. 2009, *ApJ*, 707, L1
Buitrago, F., Trujillo, I., Conselice, C. J., Bouwens, R. J., Dickinson, M., & Yan, H. 2008, *ApJ*, 687, L61
Bullock, J. S., Dekel, A., Kolatt, T. S., Kravtsov, A. V., Klypin, A. A., Porciani, C., & Primack, J. R. 2001, *ApJ*, 555, 240
Buser, R., Rong, J., & Karaali, S. 1999, *A&A*, 348, 98
Callegari, S., Mayer, L., Kazantzidis, S., Colpi, M., Governato, F., Quinn, T., & Wadsley, J. 2009, *ApJ*, 696, L89
Chiba, M., & Beers, T. C. 2001, *ApJ*, 549, 325
de Rijcke, S., Michielsen, D., Dejonghe, H., Zeilinger, W. W., & Hau, G. K. T. 2005, *A&A*, 438, 491
di Matteo, P., Combes, F., Melchior, A.-L., & Semelin, B. 2007, *A&A*, 468, 61
Dubinski, J. 1994, *ApJ*, 431, 617
Elmegreen, B. G., & Elmegreen, D. M. 2006, *ApJ*, 650, 644
Ferguson, A. M. N., Irwin, M. J., Ibata, R. A., Lewis, G. F., & Tanvir, N. R. 2002, *AJ*, 124, 1452
Ferguson, A. M. N., Johnson, R. A., Faria, D. C., Irwin, M. J., Ibata, R. A., Johnston, K. V., Lewis, G. F., & Tanvir, N. R. 2005, *ApJ*, 622, L109
Font, A. S., Navarro, J. F., Stadel, J., & Quinn, T. 2001, *ApJ*, 563, L1
Forbes, D. A., Beasley, M. A., Bekki, K., Brodie, J. P., & Strader, J. 2003, *Science*, 301, 1217
Gauthier, J.-R., Dubinski, J., & Widrow, L. M. 2006, *ApJ*, 653, 1180

- Girard, T. M., Korchagin, V. I., Casetti-Dinescu, D. I., van Altena, W. F., López, C. E., & Monet, D. G. 2006, *AJ*, 132, 1768
- Governato, F., Willman, B., Mayer, L., Brooks, A., Stinson, G., Valenzuela, O., Wadsley, J., & Quinn, T. 2007, *MNRAS*, 374, 1479
- Hayashi, H., & Chiba, M. 2006, *PASJ*, 58, 835
- Helmi, A., White, S. D. M., de Zeeuw, P. T., & Zhao, H. 1999, *Nature*, 402, 53
- Hetznecker, H., & Burkert, A. 2006, *MNRAS*, 370, 1905
- Hopkins, P. F., Hernquist, L., Cox, T. J., Younger, J. D., & Besla, G. 2008, *ApJ*, 688, 757
- Huang, S., & Carlberg, R. G. 1997, *ApJ*, 480, 503
- Ibata, R., Irwin, M., Lewis, G., Ferguson, A. M. N., & Tanvir, N. 2001a, *Nature*, 412, 49
- Ibata, R., Lewis, G. F., Irwin, M., Totten, E., & Quinn, T. 2001b, *ApJ*, 551, 294
- Ibata, R., Martin, N. F., Irwin, M., Chapman, S., Ferguson, A. M. N., Lewis, G. F., & McConnachie, A. W. 2007, *ApJ*, 671, 1591
- Ibata, R. A., Gilmore, G., & Irwin, M. J. 1994, *Nature*, 370, 194
- Ivezić, Ž., et al. 2008, *ApJ*, 684, 287
- Jurić, M., et al. 2008, *ApJ*, 673, 864
- Kalirai, J. S., Guhathakurta, P., Gilbert, K. M., Reitzel, D. B., Majewski, S. R., Rich, R. M., & Cooper, M. C. 2006, *ApJ*, 641, 268
- Kazantzidis, S., Bullock, J. S., Zentner, A. R., Kravtsov, A. V., & Moustakas, L. A. 2008, *ApJ*, 688, 254
- Kazantzidis, S., Kravtsov, A. V., Zentner, A. R., Allgood, B., Nagai, D., & Moore, B. 2004, *ApJ*, 611, L73
- Kazantzidis, S., Zentner, A. R., Kravtsov, A. V., Bullock, J. S., & Debattista, V. P. 2009, *ApJ*, 700, 1896
- Kazantzidis, S., et al. 2005, *ApJ*, 623, L67
- Khochfar, S., & Burkert, A. 2006, *A&A*, 445, 403
- Layden, A. C., Hanson, R. B., Hawley, S. L., Klemola, A. R., & Hanley, C. J. 1996, *AJ*, 112, 2110
- Majewski, S. R., Skrutskie, M. F., Weinberg, M. D., & Ostheimer, J. C. 2003, *ApJ*, 599, 1082
- Malin, D., & Hadley, B. 1997, *Publications of the Astronomical Society of Australia*, 14, 52
- Martínez-Delgado, D., Butler, D. J., Rix, H.-W., Franco, V. I., Peñarrubia, J., Alfaro, E. J., & Dinescu, D. I. 2005, *ApJ*, 633, 205
- Matthews, L. D. 2000, *AJ*, 120, 1764
- Mayer, L., Governato, F., & Kaufmann, T. 2008, *Invited Review in "Advanced Science Letters"* (astro-ph/0801.3845)
- Mo, H. J., Mao, S., & White, S. D. M. 1998, *MNRAS*, 295, 319
- Moster, B. P., Maccio', A. V., Somerville, R. S., Johansson, P. H., & Naab, T. 2009, *MNRAS* submitted (astro-ph/0906.0764)
- Naab, T., & Ostriker, J. P. 2006, *MNRAS*, 366, 899
- Navarro, J. F., Frenk, C. S., & White, S. D. M. 1997, *ApJ*, 490, 493
- Newberg, H. J., et al. 2002, *ApJ*, 569, 245
- Peng, E. W., Ford, H. C., Freeman, K. C., & White, R. L. 2002, *AJ*, 124, 3144
- Pohlen, M., Balcells, M., Lütticke, R., & Dettmar, R.-J. 2004, *A&A*, 422, 465
- Purcell, C. W., Kazantzidis, S., & Bullock, J. S. 2009, *ApJ*, 694, L98
- Quinn, P. J., & Goodman, J. 1986, *ApJ*, 309, 472
- Quinn, P. J., Hernquist, L., & Fullagar, D. P. 1993, *ApJ*, 403, 74
- Read, J. I., Lake, G., Agertz, O., & Debattista, V. P. 2008, *ArXiv e-prints*, 803
- Reid, N., & Majewski, S. R. 1993, *ApJ*, 409, 635
- Sellwood, J. A., Nelson, R. W., & Tremaine, S. 1998, *ApJ*, 506, 590
- Shang, E., et al. 1998, *ApJ*, 504, L23
- Sharma, S., & Steinmetz, M. 2005, *ApJ*, 628, 21
- Soubiran, C., Bienaymé, O., & Siebert, A. 2003, *A&A*, 398, 141
- Spitzer, L. J. 1942, *ApJ*, 95, 329
- Stadel, J. G. 2001, *PhD thesis*
- Tormen, G. 1997, *MNRAS*, 290, 411
- Tóth, G., & Ostriker, J. P. 1992, *ApJ*, 389, 5
- Vallenari, A., Pasetto, S., Bertelli, G., Chiosi, C., Spagna, A., & Lattanzi, M. 2006, *A&A*, 451, 125
- Velázquez, H., & White, S. D. M. 1999, *MNRAS*, 304, 254
- Veltz, L., Bienaymé, O., Freeman, K. C., & and collaborators. 2008, *A&A*, 480, 753
- Villalobos, Á., & Helmi, A. 2008, *MNRAS*, 391, 1806
- . 2009, *MNRAS*, 399, 166
- Vitvitska, M., Klypin, A. A., Kravtsov, A. V., Wechsler, R. H., Primack, J. R., & Bullock, J. S. 2002, *ApJ*, 581, 799
- Wainscoat, R. J., Freeman, K. C., & Hyland, A. R. 1989, *ApJ*, 337, 163
- Walker, I. R., Mihos, J. C., & Hernquist, L. 1996, *ApJ*, 460, 121
- White, S. D. M., & Rees, M. J. 1978, *MNRAS*, 183, 341
- Yanny, B., et al. 2000, *ApJ*, 540, 825
- Yoachim, P., & Dalcanton, J. J. 2005, *ApJ*, 624, 701
- . 2006, *AJ*, 131, 226
- Zeldovich, Y. B., Klypin, A. A., Khlopov, M. Y., & Chechetkin, V. M. 1980, *Sov. J. Nucl. Phys.*, 31, 664